AD-A042 647 ILLINOIS UNIV AT URBANA-CHAMPAIGN COORDINATED SCIENCE LAB F/G 20/14
A SPECTRAL DOMAIN ANALYSIS OF HIGH FREQUENCY DIFFRACTION PROBLE--ETC(U)
MAY 77 Y RAHMAT-SAMII, R MITTRA DAAB07-72-C-0259
UNCLASSIFIED R-770 NL

| OF |
AD
A042647

END
DATE
FILMED
8-77
DDC

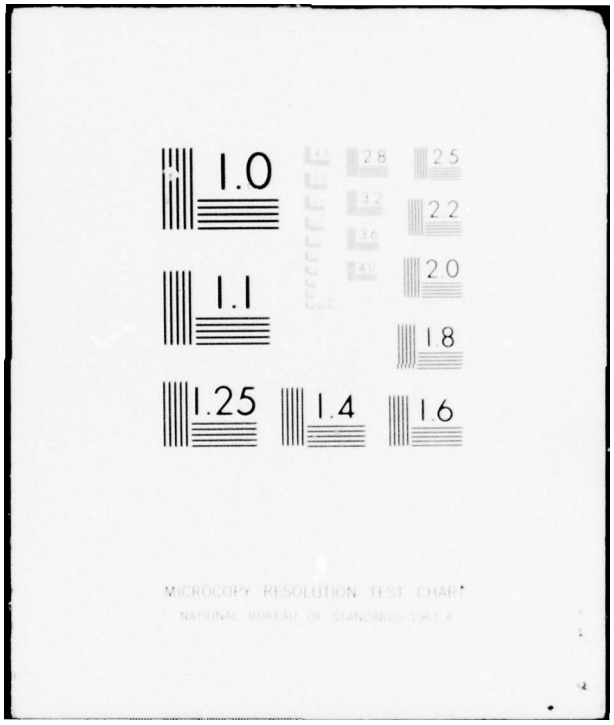
1.0
1.1
1.25
1.4
1.6
2.8
2.5
3.2
2.2
3.6
2.0
4.0
1.8
MICROCOPY RESOLUTION TEST CHART
NATIONAL BUREAU OF STANDARDS-1963-A

REPORT R-770 MAY, 1977 UILU-ENG 77-2217

COORDINATED SCIENCE LABORATORY

12

A SPECTRAL DOMAIN ANALYSIS OF HIGH FREQUENCY DIFFRACTION PROBLEMS

Y. RAHMAT-SAMII
R. MITTRA

UNIVERSITY OF ILLINOIS - URBANA, ILLINOIS

UNCLASSIFIED

SECURITY CLASSIFICATION OF THIS PAGE (When Data Entered)

REPORT DOCUMENTATION PAGE	READ INSTRUCTIONS BEFORE COMPLETING FORM
1. REPORT NUMBER (14) R-770, 2. GOVT ACCESSION NO. UILU-ENG-77-2217	3. RECIPIENT'S CATALOG NUMBER
4. TITLE (and Subtitle) A SPECTRAL DOMAIN ANALYSIS OF HIGH FREQUENCY DIFFRACTION PROBLEMS,	5. TYPE OF REPORT & PERIOD COVERED (9) Technical Report,
	6. PERFORMING ORG. REPORT NUMBER
7. AUTHOR(s) (10) Y. Rahmat-Samii and R. Mittra	8. CONTRACT OR GRANT NUMBER(s) (15) DAAB-07-72-C-0259, NSF-ENG-76-08305
9. PERFORMING ORGANIZATION NAME AND ADDRESS (2) Coordinated Science Laboratory, University of Illinois at Urbana-Champaign, Urbana, Illinois 61801	10. PROGRAM ELEMENT, PROJECT, TASK AREA & WORK UNIT NUMBERS
11. CONTROLLING OFFICE NAME AND ADDRESS Joint Services Electronics Program	12. REPORT DATE (11) May, 1977
	13. NUMBER OF PAGES ~~80~~ (12) 86p.
14. MONITORING AGENCY NAME & ADDRESS (if different from Controlling Office)	15. SECURITY CLASS. (of this report) UNCLASSIFIED
	15a. DECLASSIFICATION/DOWNGRADING SCHEDULE

16. DISTRIBUTION STATEMENT (of this Report)

Approved for public release; distribution unlimited

17. DISTRIBUTION STATEMENT (of the abstract entered in Block 20, if different from Report)

18. SUPPLEMENTARY NOTES

19. KEY WORDS (Continue on reverse side if necessary and identify by block number)

High-Frequency Diffraction
Spectral Analysis
Half-Plane Diffraction
Arbitrary Illumination

20. ABSTRACT (Continue on reverse side if necessary and identify by block number)

This report studies the application of spectral domain analysis to the problem of the high-frequency diffraction of electromagnetic waves. ~~We first summarize~~ the basic formulation of the spectral approach is first summarized and then ~~apply it~~ applied in a unified fashion to the important problems of the non-uniform illumination of a half-plane and staggered parallel planes. Special attempts are made to analytically determine the fields at the shadow boundaries and numerically evaluate them in the transition regions. Comparison is made with other high-fequency asymptotic techniques and some unique conclusions are obtained. → next page

DD FORM 1 JAN 73 1473 EDITION OF 1 NOV 65 IS OBSOLETE

UNCLASSIFIED

SECURITY CLASSIFICATION OF THIS PAGE (When Data Entered)

097 700

Furthermore, it is shown that the important task of testing and improving high-frequency solutions can be accomplished by employing the Fourier transform of the integral equation for the surface current and using Galerkin's method in the spectral domain. Some examples of this approach are also included.

UILU-ENG 77-2217

A SPECTRAL DOMAIN ANALYSIS OF HIGH FREQUENCY DIFFRACTION PROBLEMS

by

Y. Rahmat-Samii and R. Mittra

This work was supported in part by the Joint Services Electronics Program (U.S. Army, U.S. Navy and U.S. Air Force) under Contract DAAB-07-72-C-0259 and in part by the National Science Foundation under Grant NSF-ENG-76-08305.

A SPECTRAL DOMAIN ANALYSIS OF HIGH FREQUENCY DIFFRACTION PROBLEMS

Y. Rahmat-Samii and R. Mittra

Coordinated Science Laboratory
and
Electromagnetics Laboratory
of the
Department of Electrical Engineering
University of Illinois at Urbana-Champaign
Urbana, Illinois

Key Words:

High-Frequency Diffraction

Spectral Analysis

Half-plane Diffraction

Arbitrary Illumination

Asymptotic Techniques

Uniform Theories

Shadow Boundaries

Transition Regions

Staggered Parallel Plates

Integral Equation in Spectral Domain

Scattering by Cylinders

ABSTRACT

This report studies the application of spectral domain analysis to the problem of the high-frequency diffraction of electromagnetic waves. We first summarize the basic formulation of the spectral approach and then apply it in a unified fashion to the important problems of the non-uniform illumination of a half-plane and staggered parallel planes. Special attempts are made to analytically determine the fields at the shadow boundaries and numerically evaluate them in the transition regions. Comparison is made with other high-frequency asymptotic techniques and some unique conclusions are obtained.

Furthermore, it is shown that the important task of testing and improving high-frequency solutions can be accomplished by employing the Fourier transform of the integral equation for the surface current and using Galerkin's method in the spectral domain. Some examples of this approach are also included.

1. INTRODUCTION

Ever since Keller's pioneering work [1] on the Geometrical Theory of Diffraction (GTD), representing an extension of Geometrical optics (GO), there has been a tremendous amount of progress made toward the development of the concepts of ray methods and their application to high-frequency diffraction problems. One of the principal attributes of the ray techniques is that they exploit the "local" nature of the field solution at high frequencies. The principle of the local field states that the high-frequency limit processes such as reflection and diffraction depend only on the local geometrical and electrical properties of the scatterer in the immediate neighborhood of the point of reflection and diffraction [2]. This concept is extremely useful as it allows one to construct the solution for the scattered field from a complicated geometry by isolating the so-called scattering centers, to compute their individual contributions from the knowledge of the scattering properties of associated canonical geometries, and finally to sum these contributions to generate the total field.

Although the ray methods based on Keller's theory work remarkably well for a very wide class of high-frequency diffraction problems, there are situations where the need for refining these solutions becomes clearly evident. A few examples of such situations are: (i) the observation point at which the scattered field is desired is located at the incident or reflection shadow boundary of a diffracted edge; (ii) a second diffracting edge is located at the shadow boundary of the first edge; and (iii) near end-on incidence of a single or multiple-edged structure, e.g., a strip or an open-ended cylinder. Various approaches based on so-called uniform theories or equivalent current methods have been proposed and extensively

developed with the purpose of circumventing the difficulties in Keller's theory. Typically, they attempt to preserve the spirit of Keller's ray concepts and correct it postfact with some modifications of the original formulas at the "trouble regions."

In this communication the authors develop an alternate interpretation of the high-frequency diffraction phenomenon which is based on the concepts of "spectral domain" [3]. In this method the scattered far fields are viewed as the Fourier transform of the induced current on the scatterer and are thus associated with the spectrum of the surface current distribution. Some significant advantages accrue from the use of the spectral domain concepts for the derivation of the solution of high-frequency diffraction problems. First, we show that the spectral concept yields results identical to Keller's formulas where they apply, but the formulas based on spectral concepts continue to be valid at shadow boundaries, and caustic regions, and for edge-edge interactions, etc., where Keller's formula runs into difficulty. Second, we demonstrate that the spectral formulation can be used in a very systematic fashion to produce the higher order asymptotic terms for some important cases. Finally, we show that the important task of testing and systematically improving high frequency solutions, whether derived by ray methods or spectral techniques, can be accomplished by working with the Fourier transform of the integral equation for the surface current and by using iteration or Galerkin's method in the spectral domain.

Illustrative examples and comparison with other contemporary techniques for solving similar high-frequency diffraction problems are liberally included in the paper to show the ease of application and the systematic nature of the spectral concept and its usefulness for handling practical problems.

2. DIFFRACTION OF A PLANE WAVE BY A HALF-PLANE

The problem of plane-wave diffraction by a half-plane has been analyzed extensively in the literature since Sommerfeld's well-known solution in 1896. The reader may refer to the standard texts of Noble [4], Born and Wolf [5], Mittra and Lee [6], and others in which comprehensive reviews are found. The principal reason why the half-plane solution plays such an important role in diffraction theory is that it forms an integral part of the solution of a large class of high-frequency diffraction problems dealing with more complex bodies. In this section we re-examine this classical problem from a new angle in which the solution is constructed in the spectral domain after introducing the concept of the spectral diffraction coefficient. Only a brief discussion of the solution is presented here, mainly with the objective of laying the foundation for more complex problems to be dealt with in the following sections.

2.1 Basic Formulation

The geometry of a perfectly conducting half-plane located at $y = 0$, $x \leq 0$ and illuminated by a plane wave is shown in Fig. 1a. The Cartesian coordinates (x,y,z) and the cylindrical coordinates (ρ,ϕ,z) are erected at the edge of the half-plane. Angles are defined positively counterclockwise with the range $[-\pi,\pi]$. We let the direction of propagation of the incident plane wave be normal to the edge, i.e., $\vec{k}^i \cdot \hat{z} = 0$. This assumption changes the vector nature of the three-dimensional problem to a two-dimensional scalar problem. Furthermore, the problem may be classified as in the cases of E-wave (nonzero field components E_z, H_x, H_y), or H-wave (nonzero field components H_z, E_x, E_y) by simply letting the incident field E-field or H-field be directed alternatively along the

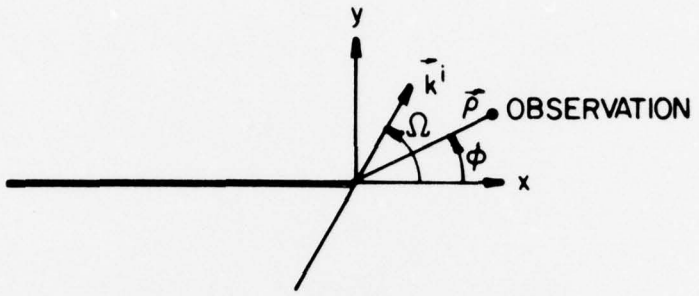

(a)

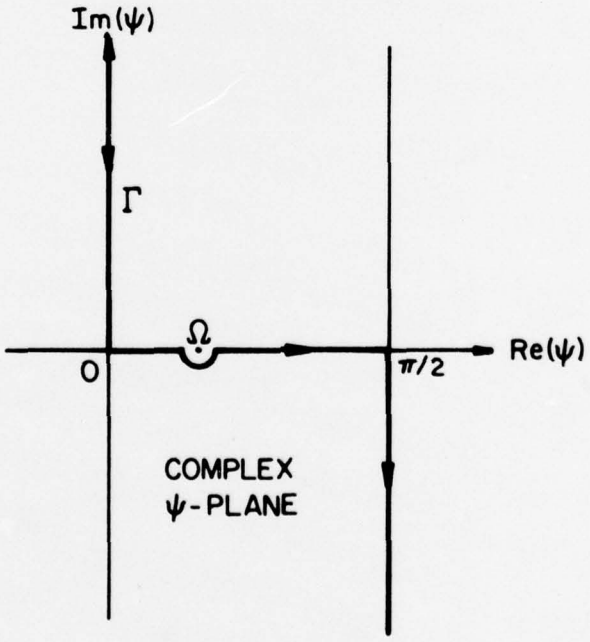

(b)

Figure 1a and b. (a) Diffraction of a plane wave by a half-plane, $0 \leq \Omega \leq \pi$ and $-\pi \leq \phi < \pi$. (b) Integration path Γ for integral representation (11).

z-axis. Unless otherwise specified, the cases of E- and H-waves are treated simultaneously, with the help of two symbols u and τ such that

$$\text{for E-waves:} \quad u = E_z \ , \ \tau = -1 \tag{1a}$$

$$\text{for H-waves:} \quad u = H_z \ , \ \tau = +1 \ . \tag{1b}$$

The total field u^t may be split into the incident field u^i and the scattered field u^s to give

$$u^t = u^i + u^s \ . \tag{2}$$

For a perfect electric conductor the total field u^t is subject to the boundary condition $u^t = 0$ or $\partial u^t/\partial y = 0$ for E-wave or H-wave cases, respectively, on the half-plane. If one defines the induced electric current on the half-plane as

$$\text{for E-wave:} \quad J_z = \left.\frac{\partial u^t}{\partial y}\right|_{0^+}^{0^-} \tag{3a}$$

$$\text{for H-wave:} \quad J_x = -\left.u^t\right|_{0^+}^{0^-} \ , \tag{3b}$$

and uses the time convention $e^{-i\omega_0 t}$, one can readily arrive at the following equations using Maxwell's equation

$$\text{for E-wave:} \quad u^s = E_z^s = i\omega_0\mu \int_{-\infty}^{0} J_z(x')g_0(k|\vec{\rho} - x'\hat{x}|)\, dx' \tag{4a}$$

$$\text{for H-wave:} \quad u^s = H_z^s = \frac{\partial}{\partial y} \int_{-\infty}^{0} J_x(x')g_0(k|\vec{\rho} - x'\hat{x}|)\, dx' \tag{4b}$$

where $k = \omega_0\sqrt{\mu\varepsilon}$, μ and ε are the permeability and permittivity of the medium, respectively, and $g_0(k\rho) = iH_0^1(k\rho)/4$ (H_0^1 is the Hankel function of first kind and zero order). The objective is to determine J_s and u^s for

the half-plane illuminated by an incident plane wave. This is done by using transform technique and employing the results given in [6].

2.2 Spectral Diffraction Coefficient and Total Field

Let us define the Fourier transform pair as

$$U(\alpha) = \int_{-\infty}^{\infty} u(x)e^{i\alpha x}\, dx = F[u(x)] \tag{5a}$$

and

$$u(x) = \int_{-\infty+i\Delta}^{\infty+i\Delta} U(\alpha)e^{-i\alpha x}\, dx = F^{-1}[U(\alpha)] \tag{5b}$$

where Δ is a small positive number. The incident plane wave may also be written as

$$u^i = e^{i\vec{k}\cdot\vec{\rho}} = e^{i(k_x x + k_y y)} = e^{ik\rho\cos(\Omega-\phi)} \tag{6}$$

where $k_x = k\cos\Omega$, $k_y = k\sin\Omega$ and $0 \leq \Omega \leq \pi$ is the incident angle shown in Fig. 1a. Transforming (4) into the spectral (Fourier) domain and applying the well-known Wiener-Hopf construction [6], one arrives at the following

$$\text{for E-wave:}\quad F[J_z] = (i\omega_0\mu)^{-1}X(k_x,\alpha) \tag{7a}$$

$$\text{for H-wave:}\quad F[J_x] = -\gamma^{-1}X(k_x,\alpha) \tag{7b}$$

where $X(k_x,\alpha)$ is

$$X(k_x,\alpha) = 2\frac{\sqrt{k+\tau k_x}\sqrt{k+\tau\alpha}}{\alpha + k_x}\ , \tag{8}$$

and $\gamma = \sqrt{\alpha^2 - k^2}$ such that Re $\gamma \geq 0$ and Im $\gamma \leq 0$, and $\alpha = k_x$. In this work, unless otherwise stated, $\sqrt{\cdot}$ and $(\cdot)^{1/2}$ are defined with their proper branch

cut slightly below the negative real axis. Using the transform version of (4) and then incorporating (7), one finally obtains

$$U^s = \begin{Bmatrix} 1 \\ \text{sgn } (y) \end{Bmatrix} X(k_x,\alpha) \frac{e^{-\gamma|y|}}{2\gamma} \quad \text{for} \begin{Bmatrix} \text{E-wave} \\ \text{H-wave} \end{Bmatrix} , \tag{9}$$

Furthermore, one may notice that the following equation has been used in the construction of (9)

$$F[g_0(k\rho)] = \frac{e^{-\gamma|y|}}{2\gamma} . \tag{10}$$

Introducing the change of variables $x = \rho \cos \phi$, $y = \rho \sin \phi$, $k_x = k \cos \Omega$, $k_y = k \sin \Omega$, $\alpha = -k \cos \psi$ and $\gamma = -ik \sin \psi$ into (9) and substituting the result into (5b), one finally arrives at

$$u^s = \frac{i}{4\pi} \begin{Bmatrix} 1 \\ \text{sgn } (\phi) \end{Bmatrix} \int_\Gamma \chi(\Omega,\psi)\, e^{ik\rho\cos(\psi-|\phi|)}\, d\psi \quad \text{for} \begin{Bmatrix} \text{E-wave} \\ \text{H-wave} \end{Bmatrix} . \tag{11}$$

In the preceding equation ψ is the complex angle defined on the path Γ, shown in Fig. 1b, and $\chi(\Omega,\psi)$ is

$$\chi(\Omega,\psi) = X(k \cos \Omega,-k \cos \psi) = \chi_i(\Omega,\psi) + \tau\chi_r(\Omega,\psi) \tag{12}$$

where

$$\chi_{\substack{i \\ r}}(\Omega,\psi) = \bar{+}\csc \frac{\Omega \bar{+} \psi}{2} . \tag{13}$$

We may notice that $\chi_i(\cdot)$ and $\chi_r(\cdot)$ have the same functional form, i.e., csc $(\cdot)$. This definition of χ_i and χ_r is closely related to the definition used by Deschamps in [7]. Clearly χ_i and χ_r are infinite at $\psi = \Omega$ and $\psi = -\Omega$, respectively. These two values of ω correspond to the incident and reflection shadow boundaries appearing in the GTD technique. As a

matter of fact, $\chi(\Omega,\psi)$ is precisely the angular part of Keller's diffraction coefficient, when ω is replaced by the observation angle ϕ. Although χ tends to infinity at the shadow boundaries, it does not mean that the field itself is also infinite as Keller's GTD predicts. Instead, the correct value of the field is obtained from (11), which is always bounded. To distinguish it from Keller's coefficient, which is associated with the diffracted field, we will refer to $\chi(\Omega,\psi)$ as the Spectral Diffraction Coefficient for the half-plane. This terminology is chosen since $\chi(\Omega,\psi)$ is associated with the spectrum, or equivalently, the Fourier transform, of the induced current and appears only inside the kernel of the plane wave spectrum representation for the field and not directly in the form of a factor multiplying the incident field as in the case of Keller's representation.

We may further use (4) and (7) and introduce the spectral coefficient of the physical optics field X_{po} as the Fourier transform of the physical optics induced current to arrive at

$$\text{for E-wave:} \quad X^{po}(k_x,\alpha) = \frac{2k_y}{\alpha + k_x} \tag{14a}$$

$$\text{for H-wave:} \quad X^{po}(k_x,\alpha) = \frac{2i\sqrt{\alpha^2 - k^2}}{\alpha + k_x} \quad . \tag{14b}$$

The application of the change of variables used in (11) allows one to express (14) as

$$\chi^{po}(\Omega,\psi) = \chi_i^{po}(\Omega,\psi) + \tau\chi_r^{po}(\Omega,\psi) \tag{15}$$

where

$$\chi_{\substack{i\\r}}^{po}(\Omega,\psi) = \mp\text{ctn}\,\frac{\Omega \mp \psi}{2} \quad . \tag{16}$$

It is worthwhile to mention that χ^f, as defined in the following equation, is bounded at the shadow boundaries

$$\chi^f(\Omega,\psi) = \chi(\Omega,\psi) - \chi^{po}(\Omega,\psi) \ . \tag{17}$$

$\chi^f(\Omega,\psi)$ could be called the fringe diffraction coefficient and it is used for the scalar aperture diffraction problems [8].

For the problem at hand, i.e., incident plane wave, the spectral integral (11) can be expressed exactly in terms of the Fresnel integral, viz.,

$$u^s = -e^{ik\rho\cos(\Omega-\phi)}F(-\xi_i) + \tau\, e^{ik\rho\cos(\Omega+\phi)}F(\xi_r) \tag{18}$$

where the Fresnel integral F is defined as

$$F(\xi) = \frac{e^{-i\pi/4}}{\sqrt{\pi}} \int_{\xi}^{\infty} e^{it^2}\, dt \tag{19}$$

and its properties are discussed in [9] and [10]. Furthermore, ξ_i and ξ_r are

$$\xi_{\substack{i\\r}} = \mp\sqrt{2k\rho}\, \sin\frac{\Omega \mp \phi}{2} \ . \tag{20}$$

Using the analytic continuation argument, one can show that, for complex angles of incidence, (18) is still the proper solution of the diffraction problem. In this context Ω is replaced by the complex angle ω which follows the path Γ_i, $[(i\infty,0)U(0,\pi)U(\pi,-i\infty)]$, in the complex ω-plane to cover the infinite spectrum of incidence angles.

In reviewing the material presented in this section, we note that its principal contribution has been the introduction of the spectral diffraction coefficient, which — in turn — is shown to be associated with the integral representation of the scattered field. The equivalence

between the GTD results and those derived from the spectral representation for observation angles not close to the shadow boundaries can be easily established by substituting the asymptotic expansion of Fresnel into (18). In the next few sections, we will illustrate the broad nature of the spectral concept and its versatility of application by considering more general incident waves and complex structures than the half-plane illuminated by a plane wave.

3. DIFFRACTION OF AN ARBITRARY INCIDENT FIELD BY A HALF-PLANE

Recently there has been much interest in the problem of predicting the characteristics of antennas mounted on complex structures, such as aircraft, and in the accurate calculation of the radiation pattern of reflector antennas used for high-frequency communication. Accurate solution of these problems requires a thorough understanding of the scattering process of an arbitrary incident field impinging on a diffracting edge. Though the problem of diffraction by a half-plane due to an incident plane wave has been studied extensively in the past, it has not been analyzed in depth for the case of an arbitrary incident field. The first rigorous mathematical treatment of the problem was given by Carslaw in 1899 where he considered the very special case of the incident field due to an isotropic line source. The latter problem was also studied by Clemmow [11], who provided much insight into the subject through the use of plane wave spectrum analysis. In his paper, Clemmow presents a good review of the existing literature up to the year 1950. A comprehensive study of the half-plane diffraction due to an incident plane wave and an isotropic line source is given in Chapter 11 of the book by Born and Wolf [5]. Khestanov [12] derived an integral representation of the field for the diffraction by an arbitrary incident field and presented a formal solution of the problem. In his construction, no details regarding the behavior of the field at the shadow boundaries were provided. Recently, Boersma and Lee [13] have employed the formalism of the Uniform Asymptotic Theory (UAT), which is based on an Ansatz developed by Ahluwalia, Lewis and Boersma [14], to obtain the asymptotic solution of the field diffracted by a half-plane due to a line source field to the order of $k^{-3/2}$ of the incident field.

Our objectives in this section are the following: (i) to present an integral representation of the incident field and study its asymptotic behavior; (ii) to derive the radiated field behavior of a multipole line source; (iii) to use spectral domain analysis (STD) in a manner discussed in the previous section and obtain a general formulation of the problem; (iv) to use asymptotic techniques and construct higher-order asymptotic expressions for the total field, including the order $k^{-5/2}$; (v) to employ numerical techniques and determine the field in the regions where asymptotic techniques cannot be used conveniently; and (vi) to compare the results with those of other asymptotic techniques and draw some unique and useful conclusions.

3.1 Incident Field-Asymptotic Expansion

3.1.1 General Case

As shown in Fig. 2a, a perfectly conducting half-plane at $x < 0$ and $y = 0$ is illuminated by an arbitrary incident field with the following spectral plane-wave representation

$$u^i(\rho_i,\phi_i) = \frac{1}{4\pi}\int_{\Gamma_i} P(\omega,k)\, e^{ik\rho_i\cos(\omega-|\phi_i|)}\, d\omega, \quad -\pi < \phi_i < \pi \tag{21}$$

where $\vec{\rho}_i = 0$ denotes the phase center for the incident field when its Fourier transform is taken along the dashed line shown in the same figure. $P(\omega,k)$ is known as the pattern function; it is assumed that this function is slowly varying in terms of a large k and has the desired differentiability property. Furthermore, the integration path Γ_i in the complex plane ω is shown in Fig. 2b and its characteristic is discussed in [6]. As a special case, if we let $P(\omega,k) = 1$, we obtain from (21)

$$u^i = \frac{1}{4} H_0^{(1)}(k\rho_i) = \frac{1}{4\pi}\int_{\Gamma_i} e^{ik\rho_i\cos(\omega-|\phi_i|)}\, d\omega \tag{22}$$

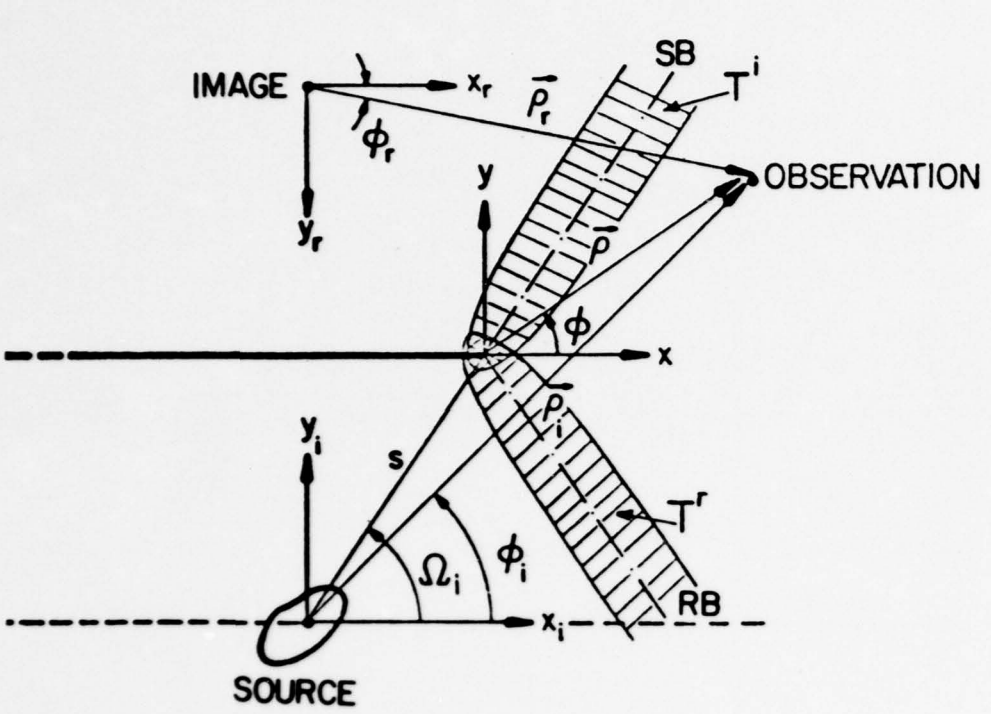

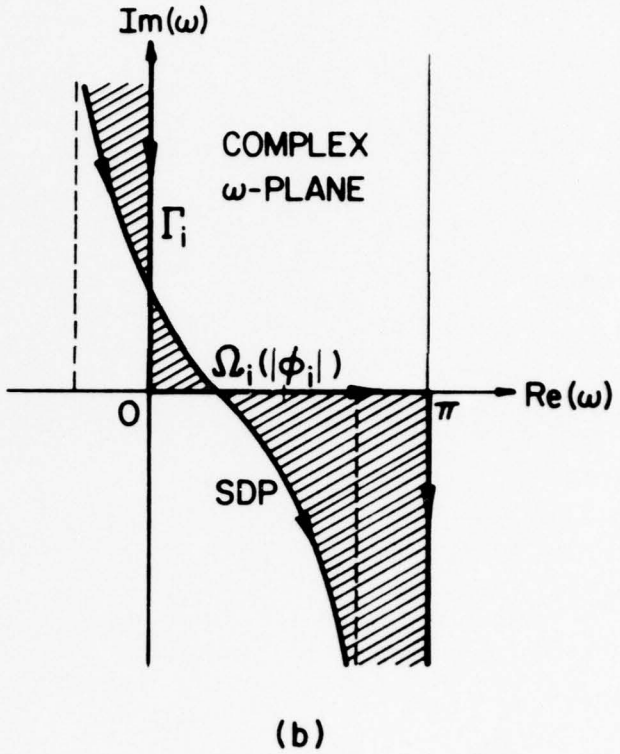

Figure 2a and b. (a) Diffraction of an arbitrary field by a half-plane. (b) Complex ω-plane, path Γ_i and steepest descent path SDP.

which is proportional to the field of an isotropic line source.

For large values of k (high frequency), one is usually interested in determining the asymptotic expression of (21). To do this, one first assumes that $P(\omega,k)$ can be expanded in terms of an asymptotic series in the following fashion

$$P(\omega,k) = \sum_{m=0}^{\infty} (ik)^{-m} P_m(\omega) \quad , \tag{23}$$

moreover, $P(\omega,k)$ does not possess any pole singularity. The path Γ_i is next deformed to the steepest descent path SDP passing through the saddle point $\omega = |\phi_i|$, as shown in Fig. 2b. On this path, the relation $\text{Re}\,[\cos(\omega - |\phi_i|)] = 1$ holds; thus one may introduce the following change of variable

$$t = \sqrt{2}\, e^{i\pi/4} \sin \frac{\omega - |\phi_i|}{2} . \tag{24}$$

in which t is a real variable taking the domain $[-\infty,\infty]$. Substituting (24) into (21) and using the fact that t is now a real variable, one finally arrives at

$$u^i(\rho_i,\phi_i) = \frac{e^{ik\rho_i + i\pi/4}}{2\sqrt{2}\pi} \int_{-\infty}^{\infty} G(t,k)\, e^{-k\rho_i t^2}\, dt \tag{25}$$

where

$$G(t,k) = P(\omega,k) \sec \frac{\omega - |\phi_i|}{2} \tag{26a}$$

in which ω is replaced by

$$\omega = 2 \text{ Arc sin } \left(\frac{e^{-i\pi/4}}{\sqrt{2}} t \right) + |\phi_i|$$

$$= \mp i \ln \left[1 + it^2 \pm (1 + i)t\sqrt{1 + it^2/2} \right] + |\phi_i|$$

$$\text{as } t \gtrless 0 \quad . \tag{26b}$$

Using (23), the asymptotic expansion of (26a) may be written as

$$G(t,k) = \sum_{m=0}^{\infty} (ik)^{-m} G_m(t) \; ; \; G_m(t) = P_m(\omega) \sec \frac{\omega - |\phi_i|}{2} \tag{27}$$

where (26b) is also implied. The complete asymptotic expansion procedure [15] is used for the asymptotic evaluation of (25). In this procedure, one first expands $G_m(t)$ in a Taylor series

$$G_m(t) = \sum_{n=0}^{\infty} \frac{G_m^{(n)}(0)}{\Gamma(n + 1)} t^n \tag{28}$$

where $G_m^{(n)}(0) = \dfrac{\partial^n}{\partial t^n} G_m(t)\Big|_{t=0}$ and Γ is the Gamma function. Then one substitutes (28) into (26a) and (25) and uses the result

$$\int_{-\infty}^{\infty} t^n e^{-k\rho t^2} dt = \begin{cases} (k\rho)^{-(1+n)/2} \Gamma[(1 + n)/2] & \text{for n even} \\ 0 & \text{for n odd} \end{cases} . \tag{29}$$

to finally arrive at

$$u^i(\rho_i, \phi_i) = \frac{e^{ik\rho_i + i\pi/4}}{2\sqrt{2\pi k}} \sum_{m=0}^{\infty} (ik)^{-m} \sum_{n=0}^{\infty} \frac{\Gamma(n + 1/2)}{\sqrt{\pi}\, \Gamma(2n + 1)} e^{in\pi/2} (ik)^{-n}$$

$$\cdot G_m^{(2n)}(0) \rho_i^{-n-1/2}$$

$$= \frac{e^{ik\rho_i + i\pi/4}}{2\sqrt{2\pi k}} \sum_{n=0}^{\infty} \frac{2^{-2n}}{n!} e^{in\pi/2} (ik)^{-n} G^{(2n)}(0,k) \rho_i^{-n-1/2} . \tag{30}$$

If we combine the order of k's in (30), we may express the incident field as

$$u^i(\rho_i,\phi_i) = \frac{e^{ik\rho_i + i\pi/4}}{2\sqrt{2\pi k}} Z^i(\rho_i,\phi_i) = \frac{e^{ik\rho_i + i\pi/4}}{2\sqrt{2\pi k}} \sum_{m=0}^{\infty} (ik)^m Z_m^i(\rho_i,\phi_i) \quad (31)$$

which has a ray field characteristic [16], i.e., satisfying the Luneberg-Kline expansion. Our task is now to determine Z_m^i's in terms of P_m's. From (27) and (26b), the following relations are easily constructed:

$$\begin{cases} G_m(0) = P_m(|\phi_i|) \\ G_m^{(1)}(0) = \left|\frac{dt}{d\omega}\right|^{-1} \frac{d}{d\omega}\left[P_m(\omega)\sec\frac{\omega - |\phi_i|}{2}\right]\Big|_{\omega=|\phi_i|} \\ \vdots \\ G_m^{(n)}(0) = D^n\left[P_m(\omega)\sec\frac{\omega - |\phi_i|}{2}\right]\Big|_{\omega=|\phi_i|} \end{cases} \quad (32)$$

where $D = \left|\frac{dt}{d\omega}\right|^{-1} \frac{d}{d\omega}$. Simplifying the above relations, one obtains

$$G_m^{(2)}(0) = -2i\left[\frac{d^2P_m(\omega)}{d\omega^2} + \frac{1}{4}P_m(\omega)\right]_{\omega=|\phi_i|} \quad (33a)$$

$$G_m^{(4)}(0) = -4\left[\frac{d^4P_m(\omega)}{d\omega^4} + \frac{5}{2}\frac{d^2P_m(\omega)}{d\omega^2} + \frac{9}{16}P_m(\omega)\right]_{\omega=|\phi_i|} . \quad (33b)$$

The higher-order terms may also be determined in the same fashion.

Substituting (33) into (30) and comparing the results with (31), we finally obtain

$$Z_0^i(\rho_i,\phi_i) = P_0(|\phi_i|)\rho_i^{-1/2} \tag{34a}$$

$$Z_1^i(\rho_i,\phi_i) = -P_1(|\phi_i|)\rho_i^{-1/2} - \left[\frac{1}{2}P_0''(|\phi_i|) + \frac{1}{8}P_0(|\phi_i|)\right]\rho_i^{-3/2} \tag{34b}$$

$$Z_2^i(\rho_i,\phi_i) = P_2(|\phi_i|)\rho_i^{-1/2} + \left[\frac{1}{2}P_1''(|\phi_i|) + \frac{1}{8}P_1(|\phi_i|)\right]\rho_i^{-3/2} + \left[\frac{1}{8}P_0''''(|\phi_i|) + \frac{5}{16}P_0''(|\phi_i|) + \frac{9}{128}P_0(|\phi_i|)\right]\rho_i^{-5/2} \tag{34c}$$

which completes the asymptotic evaluation of $u^i(\rho_i,\phi_i)$ up to and including the order of $k^{-5/2}$. We notice that the above procedure can be systematically followed to determine any higher-order terms in the asymptotic expansion of the incident field.

3.1.2 Multipole Line Source

In this section, we study the behavior of the radiated field of a multipole line source and employ the results of the previous section to construct the asymptotic expansion for the radiated field. A multipole line source, either electric or magnetic, may be defined as

$$\hat{z}J(x_i,y_i) = \hat{z}\sum_{n=0}^{N}\sum_{m=0}^{M} k^{-n-m}I_{nm}\delta^{(n)}(x_i)\delta^{(m)}(y_i) \tag{35}$$

where (n) symbolizes an nth order differentiation and I_{nm}'s are constants. The field radiated by (35) is proportional to

$$u^i(x_i,y_i) = \iint_{-\infty}^{\infty} J(x_i',y_i')\frac{i}{4}H_0^{(1)}\left[k\sqrt{(x_i - x_i')^2 + (y_i - y_i')^2}\right]dx_i'\,dy_i' \tag{36}$$

where the proportionality constant is $i\omega_0\mu$ for the electric current source (E-wave) and $i\omega_0\varepsilon$ for the magnetic current source (H-wave). Since

$$\int_{-\infty}^{\infty}\delta^{(n)}(x_i')\,e^{i\alpha x_i'}\,dx_i' = (-1)^n(i\alpha)^n \tag{37a}$$

and

$$\int_{-\infty}^{\infty} \delta^{(m)}(y_i') \frac{e^{-\sqrt{\alpha^2-k^2}|y_i-y_i'|}}{2\sqrt{\alpha^2-k^2}} dy_i' = \left(\mp\sqrt{\alpha^2-k^2}\right)^m \frac{e^{-\sqrt{\alpha^2-k^2}|y_i|}}{2\sqrt{\alpha^2-k^2}}$$

$$\text{for } y_i \gtrless 0, \tag{37b}$$

the Fourier transform of (36) along the x_i-axis may be expressed as

$$u^i(\alpha,y_i) = \int_{-\infty}^{\infty} u^i(x_i,y_i)\, e^{i\alpha x_i}\, dx_i = \left[\sum_{n=0}^{N}\sum_{m=0}^{M} k^{-n-m} I_{nm} (-i\alpha)^n \left(\mp\sqrt{\alpha^2-k^2}\right)^m\right] \cdot \frac{e^{-\sqrt{\alpha^2-k^2}|y_i|}}{2\sqrt{\alpha^2-k^2}} \quad \text{for } y_i \gtrless 0 \ . \tag{38}$$

Introducing the change of variable $\alpha = -k\cos\omega$ and $\sqrt{\alpha^2-k^2} = -ik\sin\omega$ into (38), performing the inverse Fourier transformation, and finally comparing the result with (21), we arrive at the following interpretation for the pattern function of a multipole line source

$$P(\omega,k) = P(\omega) = \sum_{n=0}^{N}\sum_{m=0}^{M} I_{nm}\, e^{i(n+m)\pi/2} (\cos\omega)^n (\operatorname{sgn}\phi_i \sin\omega)^m \ . \tag{39}$$

As expected, the pattern function of a multipole line source is independent of k. To construct the asymptotic expression of (36), one may simply use (31) and substitute $P_0(\omega) = P(\omega)$, defined in (39), into (34). It is evident that a closed-form expression for (36) may be obtained by substituting (35) into (36) and writing the final result in terms of the higher-order Hankel functions.

3.2 Diffraction by a Half-Plane

The geometry of a half-plane illuminated by an arbitrary incident field is shown in Fig. 2a. The half-plane is illuminated by an arbitrary

incident field with its plane wave spectral representation given in (21) and its pattern function in (24). The total field u^t may be split into the incident field u^i and scattered field u^s as in (22). Our goal is to determine u^s with the application of the spectral diffraction coefficient. To this end, the incident field (21) may first be expressed as

$$u^i(\rho,\phi) = \frac{i}{4\pi}\int_{\Gamma_i} P(\omega)\, e^{ik s\cos(\omega-\Omega)}\, e^{ik\rho\cos(\omega-\phi)}\, d\omega$$

$$\text{for } \rho \sin\phi > -s \sin\Omega \quad , \tag{40}$$

where s and Ω are defined in Fig. 2a. If we substitute $P(\omega) = -4\pi i\delta(\omega - \Omega)$ into (40), the plane wave (6) will be recovered. Representation (40) may be interpreted as a collection of plane waves with spectral density $i(4\pi)^{-1}P(\omega)\exp[iks\cos(\omega - \Omega)]\, d\omega$ illuminating the half-plane. Comparing (40) with (6) and using (21), one may finally express the scattered field u^s as

$$u^s = \frac{i}{4\pi}\int_{\Gamma_i} d\omega\, P(\omega)\, e^{ik s\cos(\omega-\Omega)}\left[\frac{i}{4\pi}\begin{Bmatrix} 1 \\ \text{sgn}(\phi) \end{Bmatrix}\int_{\Gamma} \chi(\omega,\psi) e^{ik\rho\cos(\psi-|\phi|)}\, d\psi\right]$$

$$\text{for } \begin{Bmatrix} \text{E-wave} \\ \text{H-wave} \end{Bmatrix}. \tag{41}$$

Attempts were made to evaluate (41) asymptotically by first replacing the Γ integration by its asymptotic expression and then calculating the Γ_i integration. Due to the nonuniform nature of this procedure, proper results could not be obtained in a convenient manner.

The inner integration over Γ in (41) may be evaluated uniformly in terms of the Fresnel integral using (21) and (18). Once this is done, one may then express u^s as

$$u^s(\rho,\phi) = u_i^s(\rho,\phi) + \tau u_r^s(\rho,\phi) \tag{42a}$$

where

$$u_{\substack{i\\r}}^s(\rho,\phi) = \frac{i}{4\pi}\int_{\Gamma_i} \mp P(\omega)\, e^{ik s\cos(\omega-\Omega)}\, e^{ik\rho\cos(\omega\mp\phi)}\, F(\mp\xi_{\substack{i\\r}})\, d\omega \quad . \tag{42b}$$

In the above equation $F(\cdot)$ has already been defined in (19) and ξ's are obtained from (20) after Ω is replaced by ω, viz.,

$$\xi_{\substack{i\\r}} = \mp\sqrt{2k\rho}\,\sin\frac{\omega \mp \phi}{2} \quad . \tag{43b}$$

It is evident that $u^s(\rho,\phi) = u^s(\rho,-\phi)$, and that (42b) can be interpreted as the superposition integral. Our task is now to evaluate (42b) asymptotically for different locations of the observation and source points according to the behavior of ξ_i and ξ_r. We first deform Γ_i to the steepest descent path SDP (see Fig. 2b) through the saddle point $\Omega = \Omega_i$ given by $\mathrm{Re}\,[\cos(\omega - \Omega)] = 1$ and $\mathrm{Im}\,[\cos(\omega - \Omega)] \geq 0$. It may be shown that the contribution of the closing segments of the integration path at infinity is zero. Since there is no pole in the integrand of (42b), this equation may be written as

$$u_{\substack{i\\r}}^s(\rho,\phi) = \frac{i}{4\pi}\int_{SDP} \mp P(\omega)\, e^{ik s\cos(\omega-\Omega)}\, e^{ik\rho\cos(\omega\mp\phi)}\, F(\mp\xi_{\substack{i\\r}})\, d\omega \quad . \tag{43}$$

Equation (43) is the starting point of our discussion for the asymptotic evaluation of the scattered field. Before dealing with this topic in the next few sections, let us introduce some definitions that will make our task convenient. Observation directions $\phi = \Omega$ and $\phi = -\Omega$ are called incident (SB) and reflection (RB) shadow boundaries,

respectively, as shown in Fig. 2a. Regions in the vicinity of SB and RB, where ξ_i and ξ_r at $\omega = \Omega$ take some given values for different $\vec{\rho}$'s, are called transition regions and are designated by T^i and T^r, respectively.

3.2.1 Total field for $\phi \notin T^i \cup T^r$

In this region, the Fresnel function in (43) is substituted by its asymptotic series from the following expression

$$F(\xi) = \theta[-\mathrm{Re}(\xi e^{-i\pi/4})] + \tilde{F}(\xi) \quad \text{for} \quad |\xi| >> 0 \tag{44a}$$

where

$$\tilde{F}(\xi) = e^{i\xi^2} \frac{e^{i\pi/4}}{2\pi\xi} \sum_{m=0}^{\infty} \Gamma(m + 1/2)(i\xi^2)^{-m} \quad , \tag{44b}$$

and θ is the unit step function. It is noticed that $\tilde{F}(\xi)$ is an odd function, i.e., $\tilde{F}(-\xi) = -\tilde{F}(\xi)$. One may then express (43) as

$$u_{\substack{i\\r}}^{s}(\rho,\phi) = u_{\substack{i\\r}}^{g}(\rho,\phi) + u_{\substack{i\\r}}^{d}(\rho,\phi) \tag{45a}$$

where

$$u_{\substack{i\\r}}^{g}(\rho,\phi) = \frac{1}{4\pi} \int_{SDP(\Omega)} \mp P(\omega)\, e^{ik s\cos(\omega-\Omega)}\, e^{ik\rho\cos(\omega\mp\phi)} \cdot \theta\left[-\mathrm{Re}\left(\mp\xi_{\substack{i\\r}} e^{-i\pi/4}\right)\right] d\omega \tag{45b}$$

and

$$u_{\substack{i\\r}}^{d}(\rho,\phi) = \frac{i\, e^{ik\rho}}{4\pi} \int_{SDP(\Omega)} P(\omega)\, e^{ik s\cos(\omega-\Omega)}\, e^{-i\xi_{\substack{i\\r}}^2} \tilde{F}(\xi_{\substack{i\\r}})\, d\omega \quad . \tag{45c}$$

Since $u_r^d(\rho,\phi) = u_i^d(\rho, 2\pi - \phi)$, our attention will only be focused on the asymptotic evaluation of u_i^d. On the SDP path, we introduce the change of variable

$$\omega = 2\,\mathrm{Arcsin}\left(\frac{e^{-i\pi/4}}{\sqrt{2}}\, t\right) + \Omega = \mp i\, \ell n\left[1 + it^2 \mp (1 + i)t\sqrt{1 + it^2/2}\right] + \Omega \quad \text{for } t \gtrless 0 \tag{46}$$

into (45c) to have the integration performed on the real line. We notice that $\cos(\omega - \Omega) = 1 + it^2$ and that both $\ell n\,[\cdot]$ and $\sqrt{\cdot}$ are defined with their branch cuts on the negative real axis. Following the same steps used in the previous section to generate (30), we arrived at

$$u_i^d(\rho,\phi) = g(ks)g(k\rho) \sum_{m=0}^{\infty} (ik)^{-m} \sum_{n=0}^{\infty} \frac{\Gamma(n + 1/2)}{\Gamma(2n + 1)} e^{in\pi/2} (ik)^{-n} G_m^{(2n)}(0)s^{-n} \tag{47}$$

where

$$g(k\rho) = \frac{e^{ik\rho + i\pi/4}}{2\sqrt{2\pi k\rho}} \quad , \tag{48}$$

and $G_m^{(2n)}$'s are obtained from (28) using

$$G_m(t) = -\frac{1}{\pi} \Gamma(m + 1/2)\ (2\rho)^{-m} \csc^{2m+1}\left(\frac{\omega - \phi}{2}\right) \sec\frac{\omega - \Omega}{2}\ P(\omega) \tag{49}$$

such that, at the same time, ω is replaced by t from (46).

The diffracted field u_i^d may be expressed as

$$u_i^d(\rho,\phi) = u_{i1}^d(\rho,\phi) + u_{i2}^d(\rho,\phi) + u_{i3}^d(\rho,\phi) + O(k^{-4}) \tag{50}$$

in which the r.h.s. of (50) is obtained by using (47) and simplifying the result. After performing all the necessary manipulations, i.e., using the same steps as in (32) and (33), we finally arrive at

$$u_{i1}^d(\rho,\phi) = g(k\rho)\chi_i g(ks)P(\Omega) \tag{51a}$$

$$u_{i2}^d(\rho,\phi) = \frac{1}{4} g(k\rho)(ik\rho)^{-1}\chi_i^3 g(ks)P(\Omega) + \frac{1}{2} g(k\rho)\left[\frac{1}{2}\chi_i^3 P(\Omega) + \cos\frac{\Omega - \phi}{2}\chi_i^2 P'(\Omega) + \chi_i P''(\Omega)\right](iks)^{-1} g(ks) \tag{51b}$$

$$u_{i3}^{d}(\rho,\phi) = \frac{3}{16}\, g(k\rho)(ik\rho)^{-2}\chi_i^5 g(ks)P(\Omega)$$
$$+ \frac{1}{8}\, g(k\rho)(ik\rho)^{-1}\left[\left(-2\chi_i^3 + 3\chi_i^5\right)P(\Omega) + 3\cos\frac{\Omega-\phi}{2}\,\chi_i^4 P'(\Omega)\right.$$
$$\left. + \chi_i^3 P''(\Omega)\right](iks)^{-1}g(ks) + \frac{1}{8}\, g(k\rho)\left[\frac{3}{2}\,\chi_i^5 P(\Omega)\right.$$
$$+ \cos\frac{\Omega-\phi}{2}\left(2\chi_i^2 + 3\chi_i^4\right)P'(\Omega) + \left(\chi_i + 3\chi_i^3\right)P''(\Omega)$$
$$\left. + 2\cos\frac{\Omega-\phi}{2}\,\chi_i^2 P'''(\Omega) + \chi_i P''''(\Omega)\right](iks)^{-2}g(ks) \qquad (51c)$$

where

$$\chi_{\substack{i\\r}} = \mp\csc\frac{\Omega \mp \phi}{2}\quad , \qquad (52)$$

as defined in (13). The diffracted field u^d may then simply be constructed by using the following relation

$$u^d(\rho,\phi) = u_i^d(\rho,\phi) + Ru_r^d(\rho,\phi) = u_i^d(\rho,\phi) + Ru_i^d(\rho,2\pi-\phi)\ . \qquad (53)$$

The expression of u_1^d is precisely Keller's GTD solution [1]. Thus, the leading term in (53) agrees exactly with the result provided by Keller's GTD for the region where such a solution is valid. In addition, our spectral analysis also provides higher-order terms whereas GTD is incapable of determining these terms. The expression for u_2^d agrees completely with the one obtained using the UAT formulation [13]. Furthermore, we have constructed u_3^d to show the ease in using spectral analysis for the systematic determination of higher-order terms.

To complete the asymptotic evaluation of u^t, defined in (2a), one must also determine $u_{\substack{i\\r}}^g$, given in (45b). First notice that

$$s\cos(\omega-\Omega) + \rho\cos(\omega \mp \phi) = \rho_{\substack{i\\r}}\cos(\omega - \phi_{\substack{i\\r}}) \qquad (54)$$

where its geometrical intepretation is shown in Fig. 2a. (ρ_i,ϕ_i) are the coordinates of the observation point seen from the source point, and (ρ_r,ϕ_r) are the coordinates of the observation point seen from the image of the source point and ϕ_r is measured positively clockwise with range $-\pi < \phi_r < \pi$. Substituting (54) into (45b), one can show that the SDP path may be deformed to the steepest descent path going through ϕ_i or ϕ_r, respectively. This deformation is valid as long as $\phi \notin T^i$ or $\phi \notin T^r$, respectively. The asymptotic evaluation of (45b) follows the same steps as used for (21) and the result takes the form (34) when P_0 is replaced by P. We therefore arrive at the following asymptotic results

$$u_i^g(\rho,\phi) = \begin{cases} -u^i(\rho_i,\phi_i) & \text{for } \Omega < \phi \notin T^i \\ 0 & \text{for } \Omega > \phi \notin T^i \end{cases} \tag{55a}$$

and

$$u_r^g(\rho,\phi) = \begin{cases} 0 & \text{for } -\Omega < \phi \notin T^r \\ u^r(\rho_r,\phi_r) & \text{for } -\Omega > \phi \notin T^r \end{cases} \tag{55b}$$

where u^r is the field radiated from the image point of the line source. Customarily, $u^i + u_i^g + Ru_r^g$ is called the geometrical field in the GTD construction of the field.

3.2.2 Total field at the shadow boundaries $\phi = \pm\Omega$

Along these directions, the solutions given in (51) diverge to infinity, because χ_i and χ_r take infinite values at $\phi = \Omega$ and $\phi = -\Omega$, respectively. To overcome this difficulty, we go back to (43) and rewrite it as follows

$$u_{i\atop r}^s(\rho,\pm\Omega) = \frac{i}{4\pi}\int_{SDP} \mp P(\omega)\, e^{ik(s+\rho)\cos(\omega-\Omega)}\, F\left\{\sqrt{2k\rho}\,\sin\frac{\omega-\Omega}{2}\right\} d\omega \; ; \tag{56}$$

(56) denotes two equations corresponding to $u_i^s(\rho,\Omega)$ and $u_r^s(\rho,-\Omega)$, respectively. It is noticed that the evaluation of $u_i^s(\rho,-\Omega)$ and $u_r^s(\rho,\Omega)$ follows the same procedures developed in the previous section and their asymptotic expansion can be obtained from (51). Introducing the change of variable (46) into (56), one readily arrives at

$$u_{\substack{i\\r}}^s(\rho,\pm\Omega) = \frac{\sqrt{2}}{4\pi} e^{ik(s+\rho)+i\pi/4} \int_{-\infty}^{\infty} \mp p(t)(1 + it^2/2)^{-1/2} F(e^{-i\pi/4}\sqrt{k\rho}\, t) \cdot e^{-k(s+\rho)t^2} dt \tag{57}$$

where $p(t) = P(\omega)$ after ω is replaced by t from (33). We then expand $p(t)(1 + it^2/2)^{-1/2}$ in terms of the Taylor series and substitute the result into (57). This equation can now be evaluated with the help of the following relations

$$I_n = \int_{-\infty}^{\infty} F(e^{-i\pi/4}\sqrt{k\rho}\, t)\, e^{-k(s+\rho)t^2}\, t^n\, dt \tag{58a}$$

$$I_{2n} = \frac{1}{2}\Gamma(n + 1/2)\, k^{-n-1/2}\, (s + \rho)^{-n-1/2} \tag{58b}$$

$$I_{2n+1} = -nk^{-1}(s + \rho)^{-1} I_{2n-1} + \frac{i}{2\sqrt{\pi}}\Gamma(n + 1/2)k^{-n-1}\, (s + \rho)^{-1}\, s^{-n}\sqrt{\rho/s}\ . \tag{58c}$$

Omitting all the intermediate steps, one can finally express (57) as follows [10]

$$\begin{aligned} u_i^s(\rho,\Omega) &= -u_r^s(\rho,-\Omega) \\ &= -\frac{1}{2} g[k(s + \rho)] \left\{ P(\Omega) + (ik)^{-1}\left[\frac{1}{2} P''(\Omega) + \frac{1}{8} P(\Omega)\right](s + \rho)^{-1} \right. \\ &\quad \left. + (ik)^{-2}\left[\frac{1}{8} P''''(\Omega) + \frac{5}{16} P''(\Omega) + \frac{9}{128} P(\Omega)\right](s + \rho)^{-2} \right\} \\ &\quad - g(ks)g(k\rho)\frac{2\rho}{\rho + s} P'(\Omega) - (ik)^{-1} g(ks)g(k\rho)\frac{\rho^2 + 3\rho s}{3s(s + \rho)^2} \\ &\quad \cdot [P'(\Omega) + P'''(\Omega)] - g(ks)g(k\rho)(ik)^{-2}\frac{15\rho s^2 + 10s\rho^2 + 3\rho^3}{30s^2(s + \rho)^3} \\ &\quad \cdot [4P'(\Omega) + 5P'''(\Omega) + P'''''(\Omega)] + O(k^{-7/2})\ . \end{aligned} \tag{59}$$

The first term in the r.h.s. of (59) can be identified with the negative of one half of the incident field when it is compared with (34) for $\phi_1 = \Omega > 0$, $P_0 = P$ and $P_1 = P_2 = 0$. The total field, defined in (2), may then be obtained by determining $u_r^s(\rho,\Omega) = u_i^s(\rho,2\pi - \Omega)$ from (45a) and (51). In (59) the terms up to and including the order of $k^{-5/2}$ do agree with the results given in [13] which used the UAT technique. It is noted that the dominant asymptotic term of the incident field is of the order $k^{-1/2}$.

3.2.3 Numerical evaluation

In the transition regions T^i and T^r, the procedures that were employed in the previous sections for deriving the asymptotic expression of the field no longer apply. In this section we discuss the numerical evaluation of the expressions for the field, viz., (21) and (42b), for observation angles that lie in these angular regions. Since the numerical procedure is not restricted to a specific angular region, we have employed it to evaluate the diffracted field for a wider range of observation angles than just the transition regions. Though these results are not ordered asymptotically in terms of powers of k, they do provide a good basis for checking the asymptotic results derived earlier.

In their present form, (21) and (42b) are not suitable for numerical integration quadratures, because of their highly oscillatory kernels. We deform their paths to the steepest descent paths and introduce the change of variables (26b) and (46), respectively, in (21) and (42b) to arrive at

$$u^1(\rho_i,\phi_i) = \frac{e^{ik\rho_i + i\pi/4}}{2\sqrt{2\pi}} \int_0^\infty \left[P(\omega)\Big|_t + P(\omega)\Big|_{-t} \right] (1 + it^2/2)^{-1/2} e^{-k\rho_i t^2}\, dt \tag{60a}$$

where ω is replaced by t from (26b) and

$$u_{\substack{i\\r}}^{s}(\rho,\phi) = \frac{e^{ik(s+\rho)+i\pi/4}}{2\sqrt{2}\pi} \int_0^{\infty} \left[\mp P(\omega)\, e^{-i\xi_{\substack{i\\r}}^2} F\left(\mp\xi_{\substack{i\\r}}\right)\Big|_t \mp P(\omega)\, e^{-i\xi_{\substack{i\\r}}^2} F\left(\mp\xi_{\substack{i\\r}}\right)\Big|_{-t} \right]$$

$$\cdot\, (1 + it^2/2)^{-1/2}\, e^{-kst^2}\, dt \qquad (60b)$$

where ω is replaced by t from (46). A sufficient condition for the integrand of (60b) to be bounded is that $s + \rho \cos(\Omega \mp \phi) > 0$, respectively, for u_i^s or u_r^s. Due to the fact that the integrands of (60a) and (60b) have smooth behaviors and decrease very rapidly for large values of t, conventional numerical integration techniques, e.g., Gauss quadratures, may be employed to evaluate the integrals with good accuracy. Some typical results obtained in this manner are shown in the next section where comparisons are made with other techniques.

3.3 Comparison with Other High-Frequency Techniques

Ever since the classic paper by Keller [1] on the Geometrical Theory of Diffraction (GTD), numerous attempts have been made toward extending the domain of GTD to regions where it predicts an infinite field and is therefore invalid. Most of the efforts in this direction have been concentrated on constructing uniform formulations, such as UTD, MSD and UAT, that overcome the difficulties of GTD at the incident and reflection shadow boundaries, and at the transition regions. The Uniform Theory of Diffraction (UTD) and its Modified Slope Diffraction (MSD) version have been introduced by Kouyoumjian, Pathak and Hwang [17],[18], and the Uniform Asymptotic Theory (UAT) has been developed by Ahluwalia, Lewis and Boersma [14]. The latter has been employed extensively by Boersma, Lee, Deschamps and Wolfe [13], [19], [16], [20] to investigate a number of problems of this type. UTD, MSD and UAT are asymptotic techniques based on individual hypotheses or Ansatz. Typically, there is no general proof available for the validity

or the completeness of these Ansatz and one has to apply them to certain test cases in order to establish their accuracy. The formulations of these asymptotic theories are reduced to the classical Sommerfeld's result when the plane wave illumination on a half-plane is considered. In fact, Sommerfeld's formulation is the basic foundation of all the different Ansatz that have been proposed to date. For more complex situations, the validity of the various asymptotic theories is typically checked against numerical results or experimental data, since analytical results are often unavailable in closed form. Even for the problem of diffraction of a half-plane illuminated by a line source possessing isotropic or nonisotropic patterns, there is no substantial check available for establishing the accuracy of the various asymptotic theories. Specifically, at the transition regions, it is not known how well these asymptotic theories compare with each other or with the exact solution.

The object of this section is to compare the aforementioned asymptotic theories with the exact solution that has been constructed using the spectral analysis presented in this paper. The comparison has been carried out, both analytically and numerically, for a wide range of observation angles including the shadow boundaries, transition regions, and at the angles away from these regions. For completeness, different source locations and pattern functions have been investigated and extensive results have been derived. In the following, we begin by reviewing briefly the nature of the formulation of each of the uniform theories, and follow this with the presentation of the results and conclusions.

3.3.1 Formulation of different theories

All the uniform asymptotic theories essentially approximate (22) and (42b) in an asymptotic sense. It is interesting to note that as yet there

is no proof available that justifies the use of these forms for arbitrary and complex situations. In all of these techniques the following is true for the total field

$$u^t(\rho,\phi) = v(\rho,\phi) + \tau v(\rho,2\pi - \phi) \tag{61}$$

where $v(\rho,\phi)$ takes different forms for different theories. For convenience of interpretation, all of the asymptotic theories are schematically represented in Fig. 3 . The notations in this figure are explained below.

We first give the expression of $v(\rho,\phi)$ for the GTD theory, which reads as follows

$$v(\rho,\phi) = u^g(\rho,\phi) + u^d(\rho,\phi) + O(k^{-3/2}) \tag{62a}$$

where

$$u^g(\rho,\phi) = \theta\left[\sin\frac{1}{2}(\Omega - \phi)\right] u^i(\rho_i,\phi_i) \tag{62b}$$

and

$$u^d(\rho,\phi) = -\csc\frac{\Omega - \phi}{2}\, g(k\rho)u^i(s,\Omega) \ . \tag{62c}$$

In the preceding equations, θ is the unit step function and

$$u^i(\rho_i,\phi_i) = g(k\rho_i)P(\phi_i) \quad , \tag{63}$$

that is, the first asymptotic term of (31). It is clear that the GTD formulation fails at the shadow boundaries, i.e., $\phi = \pm\Omega$, and their vicinities.

The UTD formulation overcomes this failure of GTD at the shadow boundaries by expressing $v(\rho,\phi)$ from (61) as

$$v(\rho,\phi) = u^g(\rho,\phi) + u^{D1}(\rho,\phi) + O(k^{-3/2}) \tag{64a}$$

where u^g is already defined in (62b) and u^{D1} is

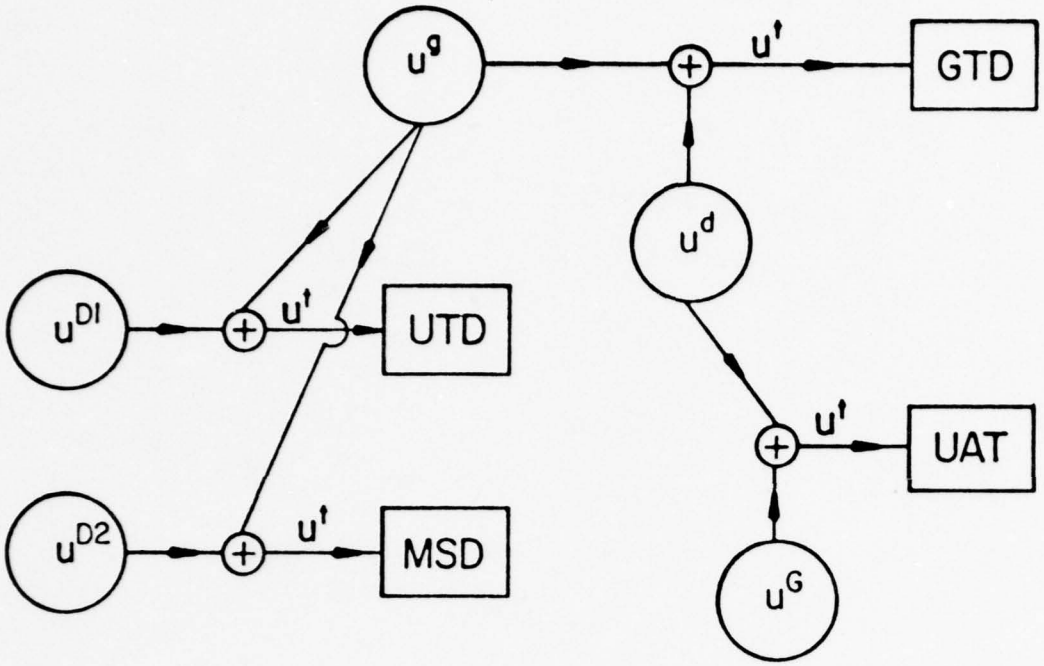

Figure 3. Schematic diagram of inherent relationships among different asymptotic techniques.

$$u^{D1}(\rho,\phi) = 2\sqrt{\pi}\ \mathrm{sgn}\left[\sin\frac{\phi-\Omega}{2}\right]\sqrt{\frac{2k\rho s}{\rho+s}}\ g(k\rho)\ e^{-i(\pi/4+\xi^2)}\ F(\xi)u^i(s,\Omega)\quad . \tag{64b}$$

In (64b) F is the Fresnel integral (26) and

$$\xi = \left|\sin\frac{\phi-\Omega}{2}\right|\sqrt{\frac{2k\rho s}{\rho+s}} \tag{64c}$$

which goes to zero at the shadow boundaries. The UTD formulation is often referred to in the literature as the Kouyoumjian-Pathak (KP) formulation.

Since UTD is only suitable for plane wave or isotropic line source types of incident field, recently a modified version of UTD that employs the notion of the slope diffraction coefficient has been introduced to generalize this procedure. This formulation, which is referred to here as MSD, modifies (64a) as

$$v(\rho,\phi) = u^g(\rho,\phi) + u^{D2}(\rho,\phi) + O(k^{-3/2}) \tag{65a}$$

where

$$u^{D2}(\rho,\phi) = u^{D1}(\rho,\phi) + \left\{2\sqrt{\pi}\ \mathrm{sgn}\left[\sin\frac{\phi-\Omega}{2}\right]\sqrt{2ks\rho}\ \rho(s+\rho)^{-3/2}\right.$$
$$\left.\cdot\ \sin(\phi-\Omega)\ e^{-i(\pi/4+\xi^2)}\ F(\xi) - 2\rho(\rho+s)^{-1}\cos\frac{\phi-\Omega}{2}\right\}$$
$$\cdot\ g(k\rho)\left.\frac{\partial u^i}{\partial\phi^i}\right|_{s,\Omega}\quad . \tag{65b}$$

In summary, UTD and its modification MSD have been introduced to modify u^d in the GTD formulation in such a manner as to cancel the discontinuity of u^g.

Finally, the Uniform Asymptotic Theory (UAT) has been invented to circumvent the shadow boundary difficulties of the GTD by writing v^t as

$$v^t(\rho,\phi) = u^G(\rho,\phi) + u^d(\rho,\phi) + O(k^{-3/2}) \tag{66a}$$

where u^d is the same term used in the GTD formulation, i.e., (61c). $U^G(\rho,\phi)$ has the form that exactly cancels the infinite value of u^d at the shadow boundaries. In this theory u^G takes the form

$$u^G(\rho,\phi) = [F(\zeta) - \hat{F}(\zeta)]u^i(\rho_i,\phi_i) \tag{66b}$$

where $\hat{F}$ is the first term of (44b)

$$\hat{F}(\zeta) = \frac{e^{i\pi/4+i\zeta^2}}{2\sqrt{\pi}\zeta} \tag{66c}$$

and ζ, which is called the detour function, is

$$\zeta = \text{sgn}\left[\sin\frac{\phi - \Omega}{2}\right]\sqrt{k[(\rho + s) - \rho_i]} \quad ; \quad \rho_i = \sqrt{s^2 + \rho^2 + 2s\rho\cos(\phi - \Omega)} \; . \tag{66d}$$

Note that at the shadow boundaries the detour ζ is zero. The higher-order asymptotic expression of UAT to the order of k^{-2} (dominant asymptotic term of u^i is $k^{-1/2}$) for the problem at hand is given by Boersma and Lee [13]. It is worth mentioning that in all of the above asymptotic techniques the field incident on the diffracting edge must be a ray field (local plane wave). Some difficulties related to the application of incident fields that do not fulfill this criterion are discussed in Section 4.

3.3.2 Numerical results and discussions

In the previous sections, some results based on analytical and numerical asymptotic evaluations of (21) and (42b) were presented for three situations — point of observation exactly at the shadow boundaries; inside the transition regions; and outside the transition regions. Additional results for this problem of diffraction of a nonisotropic line source have been given in [13]. A comparative study of the various solutions allows one to deduce certain conclusions discussed below. First, spectral

formulation (STD) can be used in a very systematic and straightforward fashion to determine any number of higher-order terms in the asymptotic expansion of the total field. In fact, by using this approach we have computed the asymptotic expression of the total field up to the order of k^{-3}. Second, UAT formulation, in its general version, can also furnish the higher-order asymptotic expression of the total field. However, in this method the higher-order terms in the diffracted field u^d must be generated through an explicit application of the edge condition. Results up to the order of k^{-2} have been reported in [13], and they agree perfectly with the STD results. Third, UTD provides the correct asymptotic expression of the field up to the order of k^{-1}, but only for an isotropic line source. Furthermore, UTD formulation does not provide higher-order asymptotic terms in a direct fashion. Finally, MSD, which is the modified version of UTD, allows one to determine the asymptotic values of the field for the unisotropic line source up to the order of k^{-1}. Again, this formulation does not provide higher-order terms in a systematic manner.

All of the above observations have been made on the basis of a comparative study of the various results directly at the shadow boundaries ($\xi = \zeta = 0$) and far away from the transition regions ($\xi >> 0, \zeta >> 0$) where the field can be expressed in a closed form. For the sake of completeness we have also investigated the behavior of the fields predicted by the various theories in the neighborhood of the transition regions. For this purpose the field integrals in STD, i.e., Eqs. (60a) and (60b), have been evaluated using an efficient numerical algorithm discussed in Section 3.2.3. Note that the computed results obtained in this manner contain all of the higher-order terms. Numerical results have also been obtained, up to the range of higher-order terms available, using GTD, UTD, MSD and UAT formulations, as given in (62a), (64a), (65a) and (66a), respectively.

In order to get better insight, we have compared both the total field u^t and the scattered field u^s, defined in (2). Some typical results are shown and discussed in the following.

Figure 4 shows the total field diffracted by a half-plane illuminated by a nonisotropic line source (E-wave) with the following pattern function obtained from (39).

$$P(\omega) = \cos \omega + \text{sgn } (\phi_i) \sin \omega \quad . \tag{67}$$

It should be noted that when (67) is used in (60b), ϕ_i is replaced by Ω and hence sgn $(\Omega) = +1$. Results are shown for different techniques and the field was sampled in a 40° angular region about the incident shadow boundary (SB^i). The SB^i direction is shown in the figure, and as expected, UTD formulation fails to provide the correct result due to the lack of proper slope discontinuity compensation. Since the incident field is well-behaved in the entire region, we have also compared the scattered field u^s for different techniques in Fig. 5. Exactly at the shadow boundaries, we can employ our higher-order asymptotic results, derived in (59) and (51), to determine the scattered field. The results of these calculations have been listed in Table 1 for different orders of k. In the same table the result of evaluation of (60b) has also been given. Though this evaluation implicitly contains all of the higher-order terms of k, the agreement with the results given in the table for terms beyond k^{-1} is remarkable. This is indeed a strong indication of the usefulness of asymptotic techniques for convenient computation of the diffracted field. We have also plotted the results tabulated in the third column of Table 1 in Fig. 5 with a view to exhibiting the behavior of the asymptotic solution. The number of terms used in the asymptotic evaluation is indicated by numerals inserted alongside the points representing the evaluation of the diffracted field at the shadow boundary.

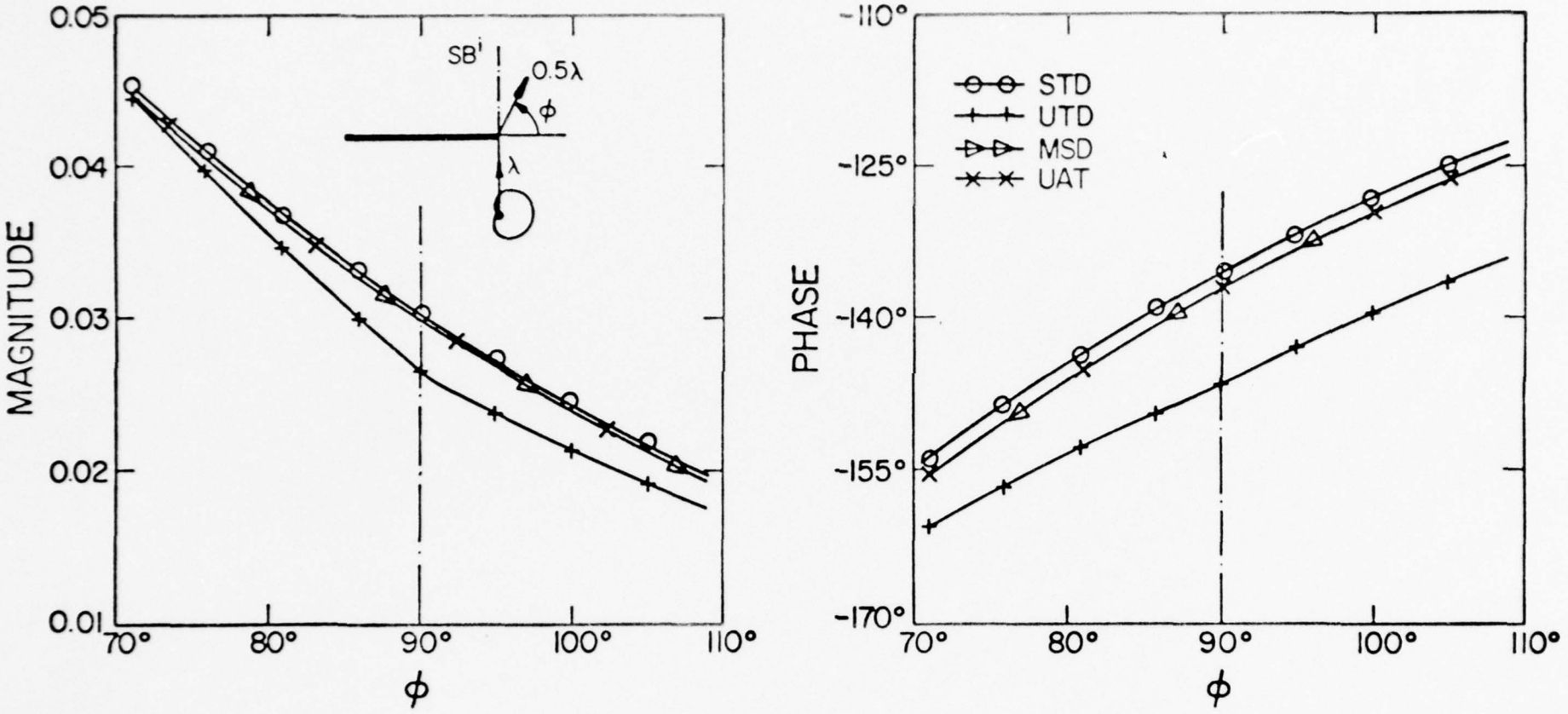

Figure 4. Total field u^t diffracted by a half-plane illuminated by a nonisotropic source (E-wave) with pattern function of (60) and $|u^i(1,\pi/2)| = .0796$.

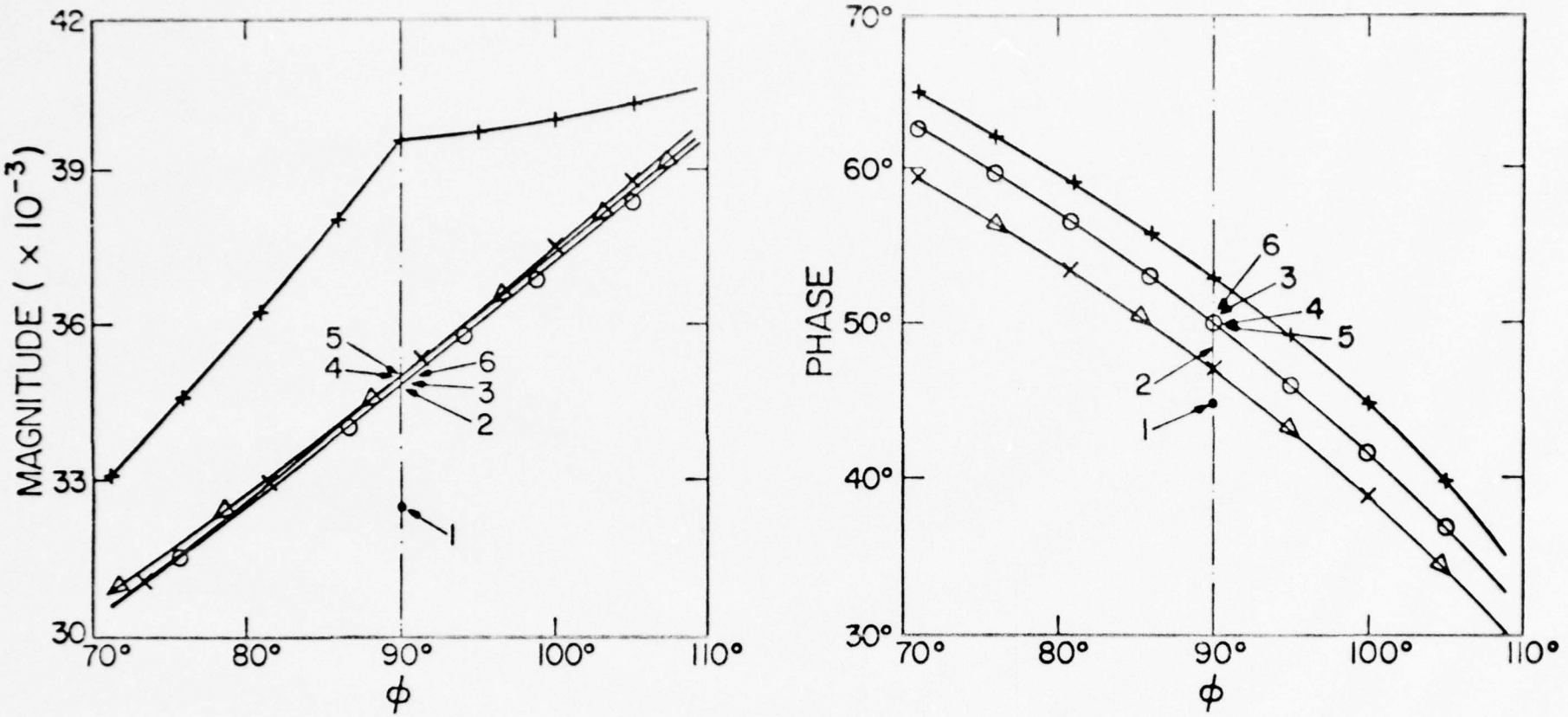

Figure 5. Scattered field u^s from a half-plane illuminated by a nonisotropic line source (Geometry shown in Figure 6). Points 1-6 are the number of terms in asymptotic expansion of u^s given in Column 3 of Table 1.

TABLE 1.

ASYMPTOTIC TERMS OF THE SCATTERED FIELD u^s EVALUATED AT THE INCIDENT SHADOW BOUNDARY (SB), SHOWN IN FIGURES 7 AND 8. FIRST COLUMN IS THE NUMBER OF TERMS, SECOND AND FOURTH COLUMNS ARE THE NUMERICAL VALUE OF EACH TERM, AND THIRD AND FIFTH COLUMNS ARE THE SUMMATION OF TERMS. THE RESULT OF THE NUMERICAL EVALUATION OF (60b) AT SB^i FOR THE NONISOTROPIC CASE IS $.034920e^{i50.11°}$.

	Nonisotropic Source, Eq. (60)		Isotropic Source	
n	$O(k^{-n/2})$	$\sum_{1}^{n}$	$O(k^{-n/2})$	$\sum_{1}^{n}$
1	$.032487e^{i45°}$	$.032487e^{i45°}$	$.032487e^{i45°}$	$.032487e^{i45°}$
2	$.002986e^{i90°}$	$.034663e^{i48.49°}$	$.008956e^{i90°}$	$.039333e^{i54.26°}$
3	$.001293e^{i135°}$	$.034766e^{i50.62°}$	$.000431e^{-i45°}$	$.039266e^{i53.64°}$
4	.000356	$.034993e^{i50.17°}$	.001069	$.039909e^{i52.41°}$
5	$.000043e^{i90°}$	$.035036e^{i50.16°}$	$.000026e^{i135°}$	$.039883e^{i52.41°}$
6	$.000184e^{i270°}$	$.034893e^{i50.66°}$	$.000326e^{-i90°}$	$.039625e^{i52.12°}$

Figure 6 displays the behavior of the scattered field calculated using the aforementioned techniques in the transition region of a half-plane illuminated by an isotropic line source (E-wave). As expected, UTD and MSD are the same and all the techniques are in very good agreement. For completeness, the asymptotic expressions have been tabulated in Table 1, and are shown in Fig. 6. Figure 7 shows the plot of the scattered field from a half-plane illuminated by an isotropic line source (E-wave) coplanar with the half-plane. For this geometry the incident and reflected shadow boundaries coincide with the half-plane itself. The scattered field was sampled in an angular region $-10° < \phi < 10°$ and results for different techniques including GTD are shown. For the sake of completeness the asymptotic results computed from (32a) are also shown in Fig. for the observation angle $\phi = 0$, and the oscillatory nature of this asymptotic solution is evident from the figure.

To further illustrate the comparative nature of the results derived from different theories, we employ the formulations of UAT, UTD, and MSD to obtain some three-dimensional representations of the total field. Figure 8, containing the geometry of the problem, is the three-dimensional plot of the total field $|u^t|$ diffracted from a half-plane illuminated by an isotropic line source (E-wave). To obtain the total field u^t, we employ the formulations of UAT and UTD, and find that essentially identical plots are obtained, although numerical values of these curves differ very slightly from each other. For instance, at the observation point $x = y = .25\lambda$, UAT and UTD formulations give $|u^t| = .05913$ and $|u^t| = .05918$, respectively. Figure 9 is the counterpart of Fig. 11 for the H-wave case. As expected, the H-field is discontinuous at the half-plane. For additional results and three-dimensional plots the reader is referred to [10].

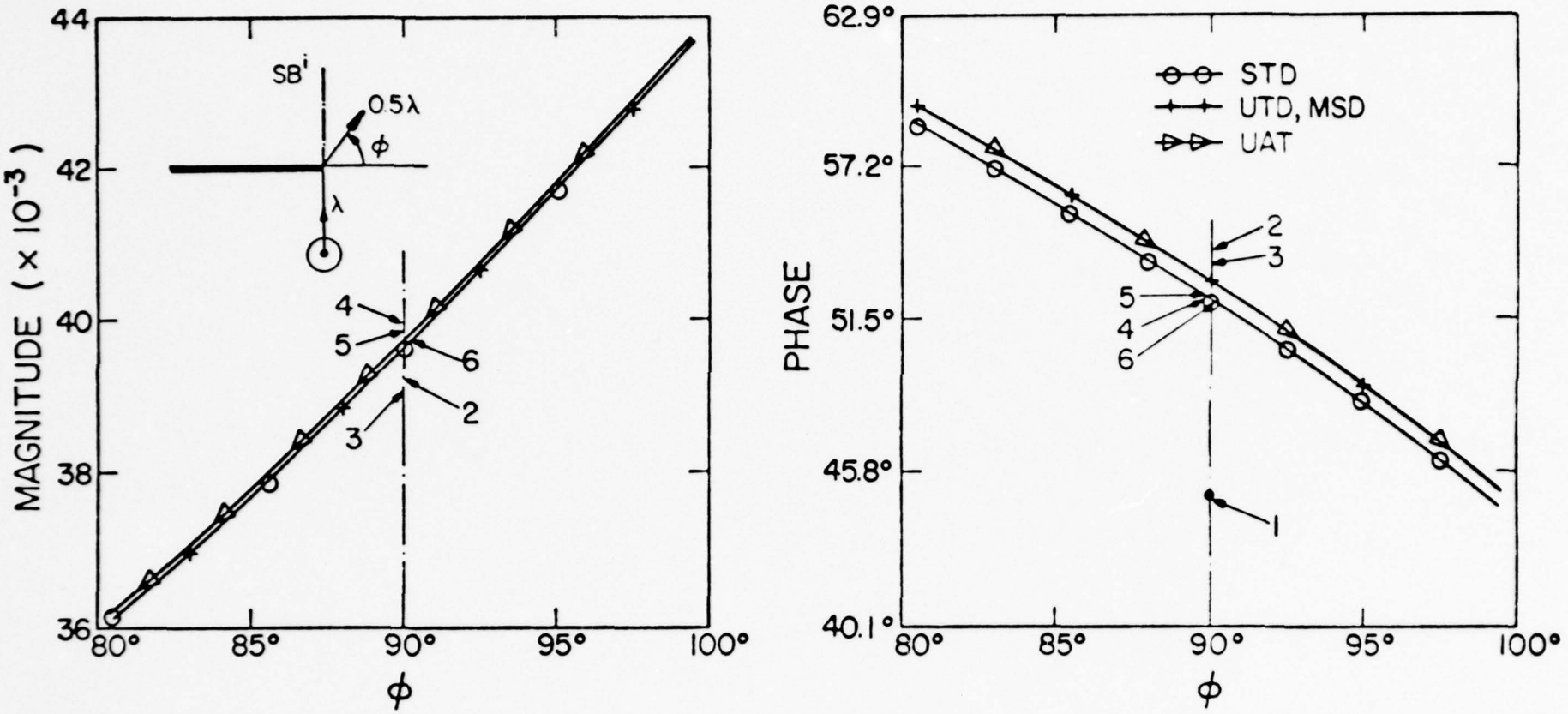

Figure 6. Scattered field u^s from a half-plane illuminated by an isotropic line source (E-wave) with $|u^i(1,\pi/2)|_s = .0796$. Points 1-6 are the number of terms in asymptotic expansion of u^s given in Column 5 of Table 1.

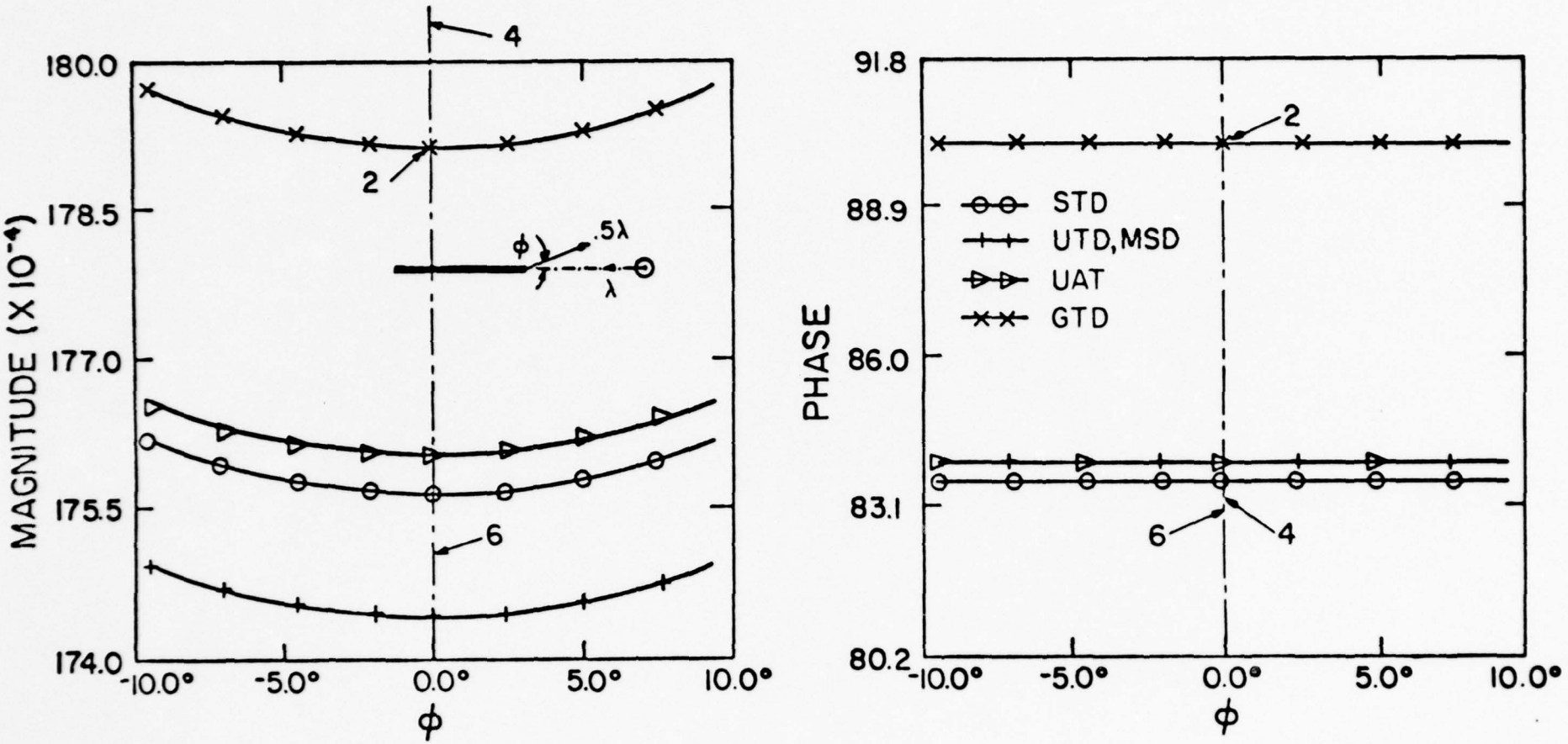

Figure 7. Scattered field u^s from a half-plane illuminated by an isotropic line source (E-wave) with $|u^i(1,\pi/2)| = .796$. Points 2, 4 and 6 are the asymptotic evaluation at $\phi = 0°$.

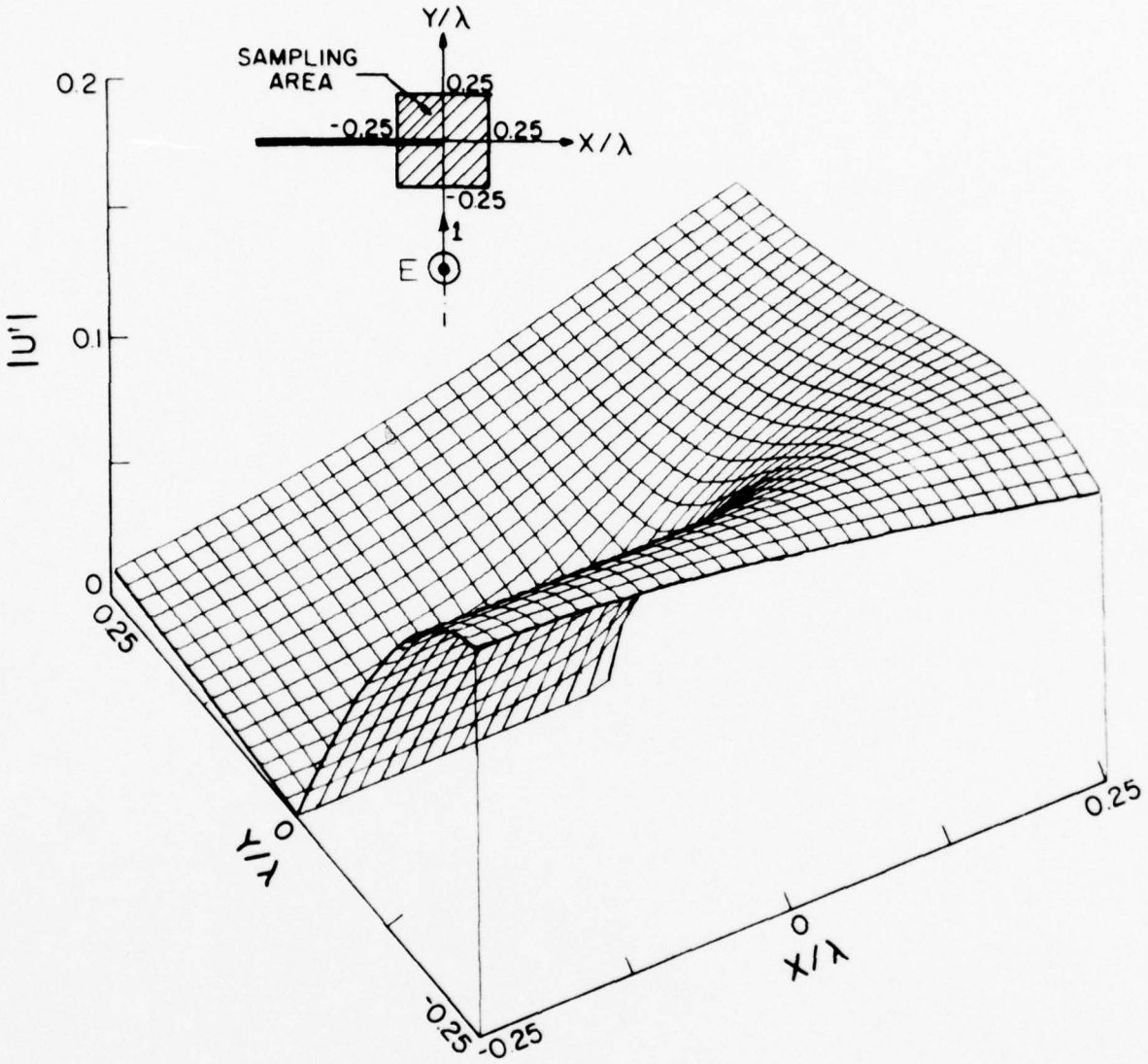

Figure 8. $|u^t|$ from UAT/UTD formulation. E-wave illumination of an isotropic source with $|u^i(1,\pi/2)| = .08$.

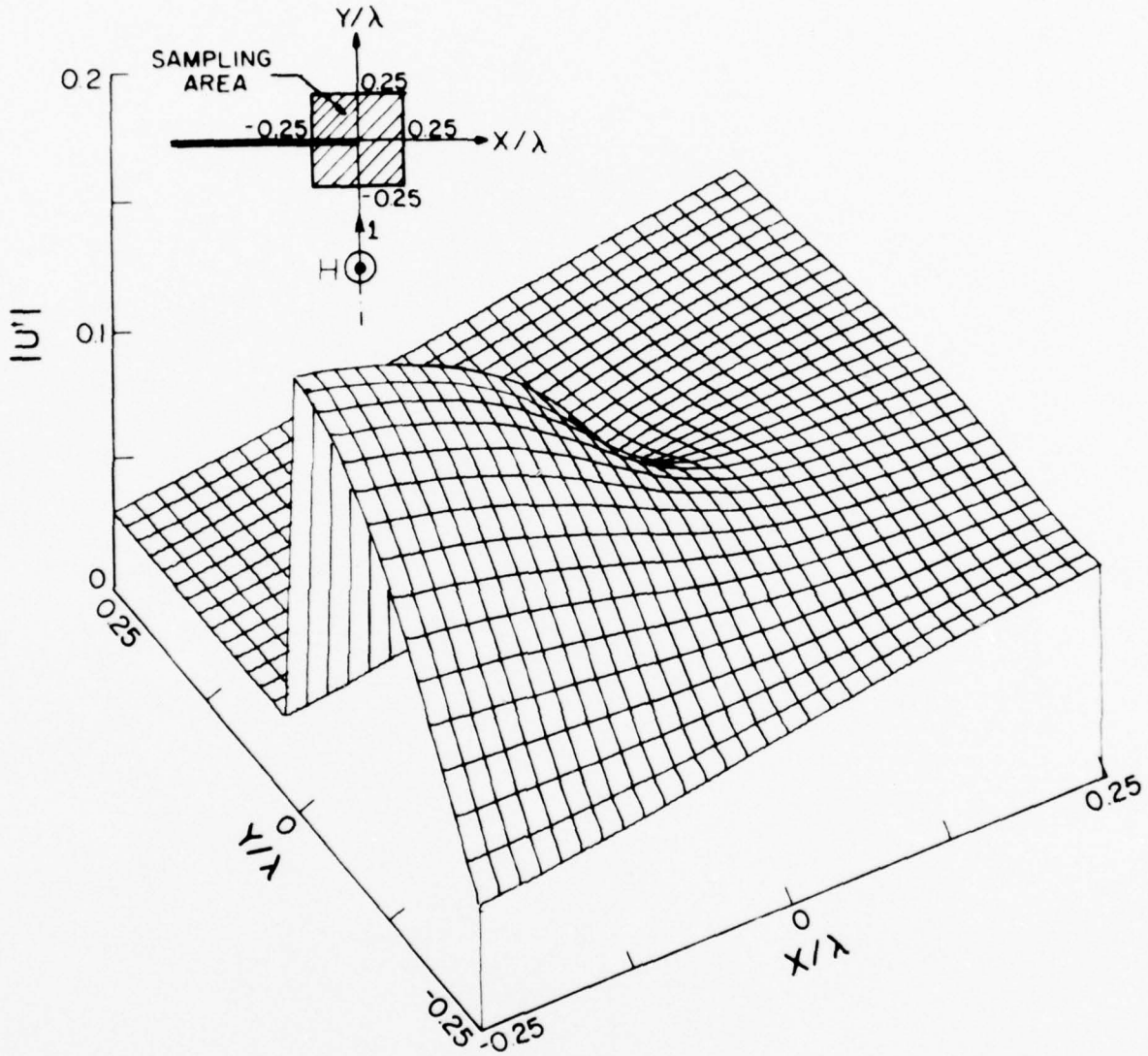

Figure 9. $|u^t|$ from UAT/UTD formulation. H-wave illumination of an isotropic source with $|u^i(1,\pi/2)| = .08$.

4. MULTIPLE-EDGE DIFFRACTION

The multiple-edge diffraction problem arises in a number of practical situations and is considerably more complicated than its single-edge counterpart. The complexity of this problem stems from the fact that the field, which impinges on the second edge after diffracting from the first, can no longer be treated, in general, as a locally uniform plane wave. It has been recognized that for the problem of diffraction by a nonplane-wave source, e.g., one with a pattern function as in Section 3, the result for the scattered field at the shadow boundaries is not just a simple modification of the plane-wave solution multiplied by the pattern function but involves the derivative of the pattern function as well. One might assume that the problem of multiple-edge diffraction can be solved by a simple extension of the pattern function illumination of a single edge. That this is not the case, however, has been pointed out by Jones [21], who has employed the Wiener-Hopf technique to construct the rigorous high-frequency expansion of the exact solution for the diffracted field by staggered parallel plates. Although Jones [21] did not explicitly obtain the results for the field at the shadow boundaries, he did examine the uniform expression he derived in some detail and concluded that the Uniform Asymptotic Theory (UAT) could not be directly (mechanically) applied at the shadow boundaries. Lee and Boersma [19] and Boersma [22] have carried out rather elaborate investigations of this problem and have shown that the UAT can still be used for this situation.

In this section, the problem of diffraction of a plane wave incident on two staggered parallel half-planes (multiple-edge) is investigated and an analysis is presented which has the following features. First, a general representation of the field after successive diffraction by two

half-planes is given in terms of a double complex integral. The analysis is carried out in the Fourier transform domain and is based on the application of the results given in Sections 2 and 3. Second, asymptotic techniques are employed to determine the total field to the order of k^{-1} in a rigorous, yet straightforward fashion for some cases of practical interest. These special cases are (see Fig. 10): (a) the edge of the top half-plane lies at or away from the shadow boundary of the bottom half-plane, i.e., the directly illuminated one; (b) the observation point lies at or away from the shadow boundary of the top half-plane. In all of these cases the final results are expressed in a compact and useful form.

4.1 Basic Formulation

The geometry of a pair of staggered, perfectly conducting, parallel half-planes illuminated by a plane wave is shown in Fig. 11. The bottom and top planes are labeled 1 and 2, respectively. The edges are separated by distance s, and the angle between the line joining the edges and the x-axis is Ω. Let the incident plane wave with unit amplitude and incident angle Ω_i take the following form at point $\vec{\rho}_1$

$$u^i(\rho_1,\phi_1) = e^{ik\rho_1\cos(\Omega_i-\phi_1)} \quad . \tag{68}$$

In this work, we neglect the interaction between planes 1 and 2, because it is assumed that s/λ is a large number. The total field diffracted by plane 1, u_1^t, may now be expressed as

$$u_1^t = u^i + u_1^s \tag{69}$$

where u_1^s is the scattered field due to the induced current in plane 1. From (11), the scattered field u_1^s can be written as

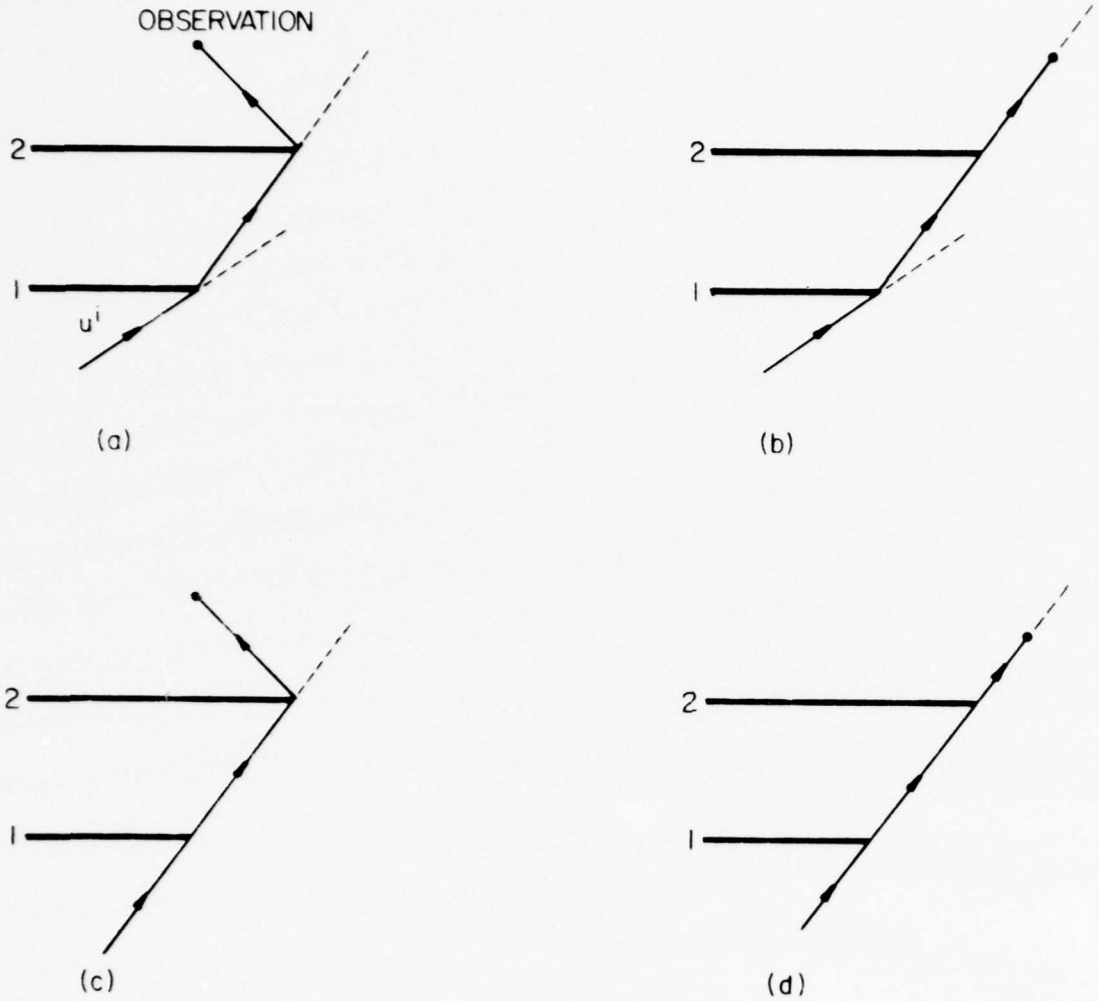

Figure 10. Relative positions of the edge of the top half-plane and the observation point with respect to the shadow boundaries.

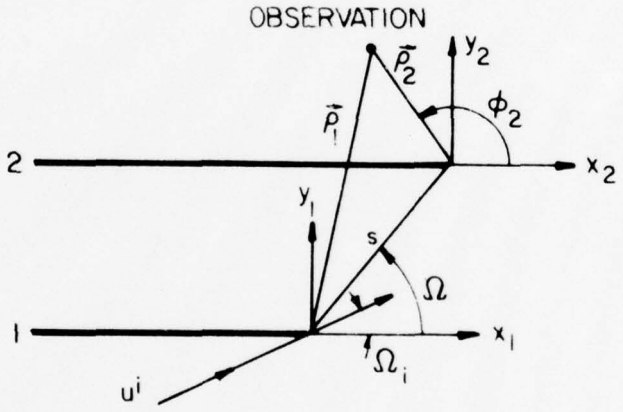

Figure 11. Diffraction of a plane wave by staggered parallel plates, $\Omega > 0$ and $\Omega_i > 0$.

$$u_1^s = \frac{i}{4\pi} \begin{Bmatrix} 1 \\ \text{sgn } (\phi_1) \end{Bmatrix} \int_{\Gamma_1} \chi(\Omega_i, \omega)\ e^{ik\rho_1 \cos(\omega - |\phi_1|)}\ d\omega$$

$$\text{for} \begin{Bmatrix} \text{E-wave} \\ \text{H-wave} \end{Bmatrix}, \tag{70}$$

where χ is defined in (12) and path Γ_1 is shown in Fig. 12a. In order to construct (70), ψ is replaced by ω in (11) for reasons which will become clear later.

Next, we consider u_1^t as the incident field impinging on the top half-plane 2. The total field diffracted by this half-plane, i.e., u_2^t, may be split into

$$u_2^t = u_1^t + u_2^s \quad , \tag{71}$$

where u_2^s is the scattered field. Since u_1^t, given in (69), consists of two parts, we may use the superposition argument and designate u_{22}^s and u_{21}^s as the scattered fields due to u^i and u_1^s, respectively. u_2^s can then be written as

$$u_2^s = u_{22}^s + u_{21}^s \quad . \tag{72}$$

The task is to determine u_2^t, which now consists of three parts as u_1^t, u_{22}^s and u_{21}^s. Fields u_1^t and u_{22}^s can be constructed from expressions given in Section 2 as they are the total and scattered fields, respectively, from the half-planes 1 and 2 illuminated by the incident plane wave (68). These fields take uniform forms similar to (18) and their asymptotic expressions can readily be derived.

In determining u_{21}^s, we compare (70) with (21) and employ equations similar to (40) and (41), arriving at

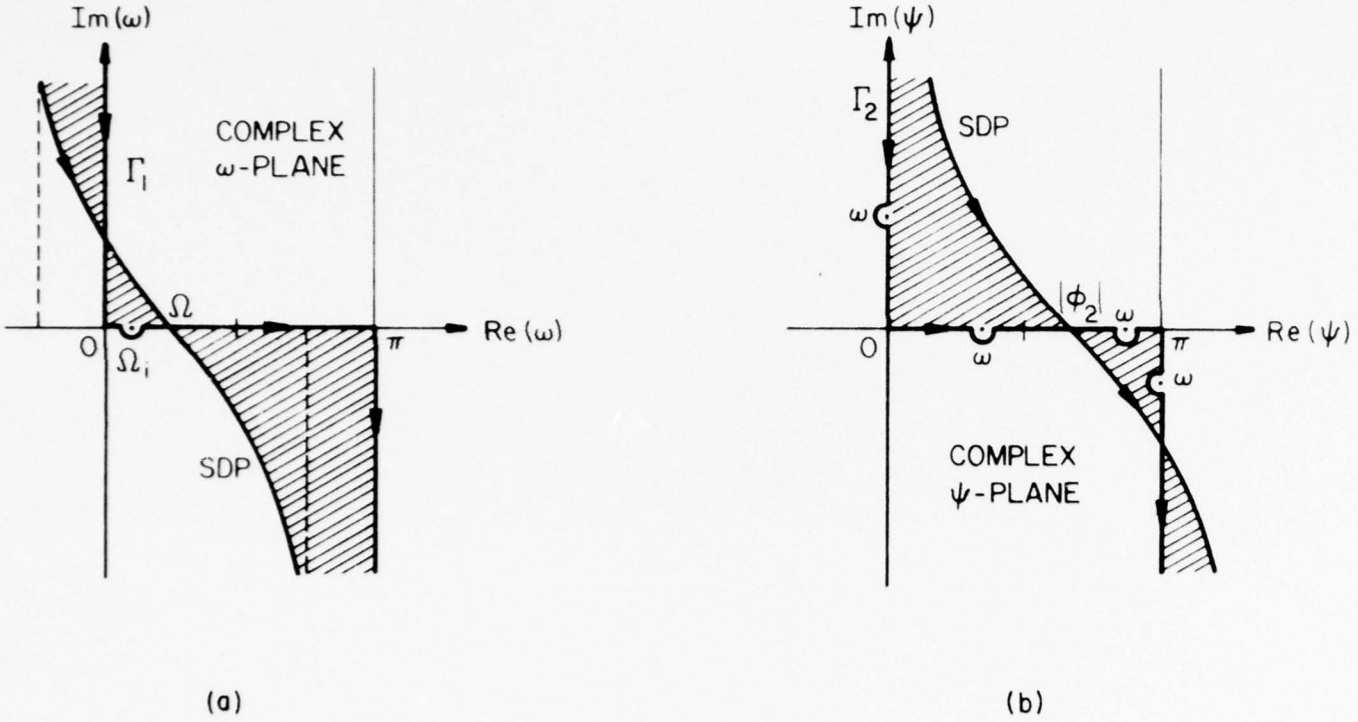

Figure 12a and b. (a) Contour Γ_1 for (70) and steepest descent path SDP for (77).
(b) Contour Γ_2^1 for (73).

$$u_{21}^{s} = \frac{i}{4\pi}\int_{\Gamma_1} d\omega\ \chi(\Omega_i,\omega)\ e^{ik\rho\cos(\omega-\Omega)}\left[\frac{i}{4\pi}\begin{Bmatrix}1\\ \mathrm{sgn}\ (\phi_2)\end{Bmatrix}\int_{\Gamma_2}\chi(\omega,\psi)e^{ik\rho_2\cos(\phi-|\phi_2|)}\ d\psi\right],$$

$$\text{for}\begin{Bmatrix}\text{E-wave}\\ \text{H-wave}\end{Bmatrix} \tag{73}$$

where ϕ_1 is replaced by $\Omega > 0$ in (70) and ρ_2 and ϕ_2 are defined in Fig. 12. Comparison of (73) with (41) reveals that $\chi(\Omega_i,\omega)$ can be interpreted as the pattern function of a fictitious line source located at the edge of half-plane 1. In contrast to $P(\omega)$, which was assumed to be regular in (41), $\chi(\Omega_i,\omega)$ is singular at $\omega = \pm\Omega_i$ and, therefore, special attention must be devoted in the asymptotic evaluation of (73). Attempts were made to first approximate the inner ψ-integral in terms of its asymptotic expansion and then to evaluate the ω-integration. Due to the nonuniform nature of this procedure, proper results could not be obtained for all the cases. Since the inner ψ-integral can be performed uniformly in terms of the Fresnel integral, we may now express (73) as

$$u_{21}^{s} = T_1 + \tau T_2 + T_3 + \tau T_4 \tag{74}$$

where

$$\begin{Bmatrix}T_1\\ 2\\ T_3\\ 4\end{Bmatrix} = \frac{i}{4\pi}\int_{\Gamma_1} \bar{+}\begin{Bmatrix}\chi_i(\Omega_i,\omega)\\ \tau\chi_r(\Omega_i,\omega)\end{Bmatrix} e^{ik\rho\cos(\omega-\Omega)} e^{ik\rho_2\cos(\omega\bar{+}\phi_2)} F(\bar{+}\xi_{\substack{i\\ r}})\ d\omega\ , \tag{75}$$

and furthermore, from (13) and (20), we have

$$\chi_{\substack{i\\ r}}(\Omega_i,\omega) = \bar{+}\csc\frac{\Omega_i \bar{+} \omega}{2} \tag{76a}$$

$$\xi_{\substack{i\\ r}} = \bar{+}\sqrt{2k\rho_2}\ \sin\frac{\omega \bar{+} \phi_2}{2}\ . \tag{76b}$$

It is noticed that on path Γ_1, χ_r is well-behaved whereas χ_i possesses a pole singularity at $\omega = \Omega_i$. Therefore, asymptotic evaluation of T_3 and T_4 follows the same steps used to evaluate (42b). In the following sections, we devote our attention to the asymptotic evaluation of T_1 and T_2, which, in conclusion, allows one to determine u_2^t from (71).

4.2 Total Field when $\Omega >> \Omega_i$ and $\phi_2 >> \Omega$ (Fig. 12a)

For this case, where the pole $\omega = \Omega_i$ and the saddle point $\omega = \Omega$ are separated, we may deform the path Γ_1 into the saddle path SDP, shown in Fig. 12a, taking into account the residue contribution of the pole $\omega = \Omega_i$, and arrive at

$$T_{\substack{1\\2}} = \frac{i}{4\pi} \int_{SDP} \mp \chi_i(\Omega_i,\omega)\, e^{ik s\cos(\omega-\Omega)} e^{ik\rho_2\cos(\omega \mp \phi_2)} F(\mp\xi_{\substack{i\\r}})\, d\omega$$
$$\pm F\left(\sqrt{2k\rho_2}\,\sin\frac{\Omega_i \mp \phi_2}{2}\right) e^{ik s\cos(\Omega_i-\Omega)}\, e^{ik\rho_2\cos(\Omega_i \mp \phi_2)}. \quad (77)$$

Since at $\omega = \Omega$ the relation $\xi_{\substack{i\\r}} \neq 0$ holds, one can then employ the results of Sec. 3.2.1 and determine the asymptotic value of (77). The same procedure can also be used to evaluate T_2 and T_3 which completes the derivation of u_{21}^s, defined in (74). Using the procedure described in connection with (71) and (72), one can also determine the asymptotic values of u_1^t and u_{11}^s. The final result for the total field u_2^t is finally given as

$$u_2^t = \chi(\Omega_i,\Omega)g(ks)\chi(\Omega,\phi_2)g(k\rho_2) + O(k^{-3/2}) \quad (78)$$

where χ and $g(\cdot)$ are defined in (12) and (48), respectively. Equation (78) agrees completely with the result obtained using GTD formulation; furthermore, $\chi(\Omega_i,\Omega)$ and $\chi(\Omega,\phi_2)$ may be identified as Keller's diffraction coefficients at the edges of half-planes 1 and 2, respectively.

4.3 Total Field when $\Omega >> \Omega_i$ and $\phi_2 = \Omega$ (Fig. 10b)

This is an interesting case, because from GTD consideration the observation angle coincides with the shadow boundary of the diffracted rays originating from half-plane 2. In this case, as in the previous case, the pole $\omega = \Omega_i$ and the saddle point $\omega = \Omega$ are separated. One can then replace T_1 and T_2 from (75) with their counterparts from (77). Since at $\omega = \Omega$ the relations $\xi_i = 0$ and $\xi_r \neq 0$ hold, evaluation of T_1 and T_3 from (77) and (75), respectively, requires special care. This is done by using the procedure described in Sec. 3.2.2. Determination of T_2 and T_4 from (77) and (75), respectively, may be completed using the analysis of Sec. 3.2.1. Finally, u_1^t and u_{11}^s can be constructed from the solution of the half-plane illuminated by a plane wave as discussed in Sec. 2. Evaluating all these components and adding them up, we finally arrive at the following total field

$$u_2^t = \frac{1}{2}\chi(\Omega_i,\Omega)g(ks + k\rho_2) + \left[\tau\chi(\Omega_i,\Omega)\chi_r(\Omega,\Omega) - \frac{2\rho_2}{\rho_2 + s}\chi'(\Omega_i,\Omega)\right] \cdot g(ks)g(k\rho_2) + O(k^{-3/2}) \tag{79}$$

where $\chi'(\Omega_i,\Omega) = \frac{\partial}{\partial\omega}\chi(\Omega_i,\omega)\Big|_{\Omega}$ and that $\phi_2 = \Omega$. Comparing the term containing χ' with the one containing P' in (59), we may once more interpret χ as the pattern function of a fictitious line source located on the edge of half-plane 1. Expression (79) can also be obtained using UAT or MSD formulations in two successive steps in a mechanical fashion from (66) and (65), respectively.

4.4 Total Field when $\Omega_i = \Omega$ and $\Omega << \phi_2$ (Fig. 10c)

This is another important case for which the edge of half-plane 1 coincides with the direction of the incident shadow boundary of the incident field. In contrast to the last two previous cases, the pole $\omega = \Omega_i$

and the saddle point $\omega = \Omega$ coincide for the situation under investigation in this section. Hence, when deforming Γ_1 into SDP for T_1 and T_2, defined in (75), the integration passes into a principal-value integral along SDP plus half the residue contribution, namely,

$$T_{\substack{1\\2}} = \frac{i}{4\pi} \int_{SDP} \bar{+} \chi_i(\Omega,\omega)\, e^{iks\cos(\omega-\Omega)} e^{ik\rho_2\cos(\omega\bar{+}\phi_2)} F(\bar{+}\xi_{\substack{i\\r}})\, d\omega$$
$$\pm \frac{1}{2} F\left(\sqrt{2k\rho_2}\sin\frac{\Omega \bar{+} \phi_2}{2}\right) e^{ik\rho_2\cos(\Omega\bar{+}\phi_2)} e^{iks} \quad . \tag{80}$$

Although at the saddle point where $\omega = \Omega$ the relation $\xi_{\substack{i\\r}} \neq 0$ holds, the procedure developed in Sec. 3.2.2 can not be used for (80) as χ_i is singular, in contrast to P which was well-behaved in (56).

The integrand of (80) is expanded in terms of Laurent series as

$$\bar{+}\chi_i(\Omega,\omega)\, e^{ik\rho_2\cos(\omega\bar{+}\phi_2)} F(\bar{+}\xi_{\substack{i\\r}}) = \frac{\bar{+}1}{\omega - \Omega} A_{\substack{i\\r}} \bar{+} B_{\substack{i\\r}} + O(\omega - \Omega) \tag{81a}$$

where

$$A_{\substack{i\\r}} = 2e^{ik\rho_2} e^{-i\xi^2_{\substack{i\\r}}} F(\bar{+}\xi_{\substack{i\\r}})\Big|_{\omega=\Omega} \tag{81b}$$

$$B_{\substack{i\\r}} = 2e^{ik\rho_2} \frac{\partial}{\partial\omega}\left[e^{-i\xi^2_{\substack{i\\r}}} F(\bar{+}\xi_{\substack{i\\r}})\right]\Big|_{\omega=\Omega} \quad . \tag{81c}$$

Substituting (81) into (80) and using saddle-point integration, we arrive at

$$T_{\substack{1\\2}} = \bar{+}B_{\substack{i\\r}} g(ks) - \frac{1}{2}\chi_{\substack{i\\r}}(\Omega,\phi_2) g(k\rho_2)\, e^{iks} + \begin{Bmatrix} 1/2 \\ 0 \end{Bmatrix} e^{ik\rho_2\cos(\Omega-\phi_2)} e^{iks}$$
$$+ O(k^{-3/2}) \tag{82}$$

where $B_{\substack{i\\r}}$ takes the following asymptotic expansion

$$B_{\substack{i\\r}} = \bar{+}2g(k\rho_2) \frac{\partial}{\partial\omega} \chi_{\substack{i\\r}}(\omega,\phi_2)\Big|_{\omega=\Omega} + O(k^{-3/2}) \quad .$$

Having determined T_1 and T_2, one can then evaluate T_3, T_4 and u_1^t and u_{11}^s in the same manner described earlier to finally arrive at

$$u_2^t = \frac{1}{2}\,\chi(\Omega,\phi_2)g(k\rho_2)\,e^{iks} + [\tau\chi_r(\Omega,\Omega)\chi(\Omega,\phi_2) + 2\chi'(\Omega,\phi_2)]\,g(ks)g(k\rho_2) + O(k^{-3/2}) \tag{83}$$

where $\chi'(\Omega,\phi_2) = \frac{\partial}{\partial\omega}\,\chi(\omega,\phi_2)\Big|_{\omega=\Omega}$. Again, the appearance of χ' is an important observation. It must be realized that for the case under study in this section, the fictitious line source interpretation does not apply anymore, because otherwise the term χ' would not have appeared in the solution. The complexity stems from the fact that the diffracted field from half-plane 1 in its shadow boundary direction is not a local plane wave.

4.5 Total Field when $\Omega_i = \Omega = \phi_2$ (Fig. 10d)

This is a unique situation as the incident direction, the observation direction, and the line connecting the edge of the half-planes are all aligned with each other. Since the pole $\omega = \Omega_i$ coincides with the saddle point $\omega = \Omega$, one can transform T_1 and T_2 from (75) into the form presented in (80). At $\omega = \Omega_i$ the relation $\xi_r \neq 0$ holds; therefore, evaluation of T_2 follows the same procedure used in Sec. 4.4 for evaluation of T_2 from (80), i.e.,

$$T_2 = -\frac{1}{2}\,\chi_r(\Omega,\Omega)g(k\rho_2)\,e^{iks} + 2\chi_r'(\Omega,\Omega)g(k\rho_2)g(ks) + O(k^{-3/2}) \quad . \tag{84}$$

Similarly, evaluation of T_3, given in (75), requires formulation of the same steps employed in Sec. 3.2.2, i.e.,

$$T_3 = \frac{-1}{2}\,\tau\chi_r(\Omega,\Omega)g[k(s+\rho_2)] - \frac{2\rho_2}{s+\rho_2}\,\tau\chi_r'(\Omega,\Omega)g(ks)g(k\rho_2) \quad . \tag{85}$$

T_4, defined in (75), may be obtained using the construction of Sec. 3.2.1 to obtain

$$T_4 = \tau\chi_r(\Omega,\Omega)g(ks)\chi_r(\Omega,\Omega)g(k\rho_2) \quad . \tag{86}$$

Since u_1^t and u_{22}^s, defined in (71) and (72), respectively, are the solutions due to plane-wave illumination of half-planes 1 and 2, respectively, one may use (18) to arrive at

$$u_1^t = \frac{1}{2}\, e^{ik(s+\rho_2)} + \tau\chi_r(\Omega,\Omega)g[k(s+\rho)] \tag{87}$$

$$u_{22}^s = -\frac{1}{2}\, e^{ik(s+\rho_2)} + \tau\chi_r(\Omega,\Omega)\, e^{iks}g(k\rho_2) \quad . \tag{88}$$

To complete our evaluation of u_2^t, the only step remaining is to determine T_1 from (80). Substituting $\phi_2 = \Omega$ into (80), one may express T_1 as

$$T_1 = \frac{i}{4\pi}\int_{SDP} -\csc\left(\frac{\omega-\Omega}{2}\right) F\left(\sqrt{2k\rho_2}\,\sin\frac{\omega-\Omega}{2}\right) e^{ik(s+\rho_2)\cos(\omega-\Omega)}\, d\omega + \frac{1}{4}\, e^{ik(s+\rho_2)} \quad . \tag{89}$$

Introducing the change of variable

$$t = \sqrt{2}\, e^{i\pi/4}\sin\frac{\omega-\Omega}{2} \tag{90}$$

into (89), one obtains

$$T_1 = \frac{1}{4}\, e^{ik(s+\rho_2)} - \frac{i}{2\pi}\, e^{ik(s+\rho_2)}\int_{-\infty}^{\infty} Q(t)F\left(e^{-i\pi/4}\sqrt{k\rho_2}\, t\right) e^{-k(s+\rho)t^2}\, dt \tag{91a}$$

where

$$Q(t) = t^{-1}(1 + it^2/2)^{-1/2} = t^{-1} - \frac{i}{4}\, t + O(t^2) \quad . \tag{91b}$$

Substituting (91b) into (91a), one notes that in addition to the integration of type (58a) with n = 1, one must also evaluate the following integral, viz.,

$$\int_{-\infty}^{\infty} F\left\{e^{-i\pi/4}\sqrt{k\rho_2}\ t\right\}\ e^{-k(s+\rho)t^2}\ t^{-1}\ dt = I(s) \quad . \tag{92}$$

Differentiation of I(s) with respect to s yields

$$\begin{aligned} I'(s) &= -k \int_{-\infty}^{\infty} F\left\{e^{-i\pi/4}\sqrt{k\rho_2}\ t\right\}\ e^{-k(s+\rho_2)t^2}\ t\ dt \\ &= -\frac{i}{2}\ (s + \rho_2)^{-1}\sqrt{\rho_2/s} \end{aligned} \tag{93}$$

for which the result given in (58a) for n = 1 is incorporated. Since $I(s) \to 0$ as $s \to \infty$, one finally obtains

$$I(s) = \frac{i}{2}\sqrt{\rho_2} \int_s^{\infty} \frac{d\sigma}{\sqrt{\sigma}\ (\sigma + \rho_2)} = i\ \tan^{-1}\sqrt{\frac{\rho_2}{s}} \ . \tag{94}$$

T_1 may at last be evaluated to yield

$$T_1 = \left(\frac{1}{4} + \frac{1}{2\pi}\ \tan^{-1}\sqrt{\frac{\rho_2}{s}}\right) e^{ik(s+\rho_2)} - \frac{\rho_2}{2(s + \rho_2)}\ g(ks)g(k\rho_2) \quad . \tag{95}$$

Now we have enough information to construct u_2^t from (71), (72) and (74), thus arriving at

$$\begin{aligned} u_2^t = e^{ik(s+\rho_2)}&\left[\frac{1}{4} + \frac{1}{2\pi}\ \tan^{-1}\sqrt{\frac{\rho_2}{s}}\right] + [g(ks + k\rho_2) + e^{iks}g(k\rho_2)] \\ &\cdot \frac{\tau}{2}\ \chi_r(\Omega,\Omega) + g(ks)g(k\rho)\left[-\frac{\rho_2}{2(s + \rho_2)} + \chi_r^2(\Omega,\Omega) + \frac{2s}{s + \rho_2}\ \tau\chi_r'(\Omega,\Omega)\right] \\ &+ O(k^{-3/2}) \quad , \end{aligned} \tag{96}$$

where

$$\chi_r(\Omega,\Omega) = \frac{1}{\sin\Omega} \quad , \quad \chi_r'(\Omega,\Omega) = -\frac{\cos\Omega}{2\sin^2\Omega} \; . \tag{97}$$

This is an important result and can not be obtained via simple application of ray techniques.

4.6 Comparison with Other Techniques

In this section, we apply the formulation of uniform techniques, discussed in Sec. 3.3.1, to the geometry of staggered parallel plates. Results obtained by a cascading approach, in which the fields scattered by the first half-plane are directly used as the incident fields for the second half-plane, are compared with those given in the previous sections using spectral analysis.

For the situation shown in Fig. 10a, where both the edge of half-plane 2 and the observation point are outside the transition regions, GTD, UTD, MSD and UAT give the same asymptotic result, and are in complete agreement with (78). This is the simplest situation for which even the GTD formulation provides an adequate result.

In the case shown in Fig. 10b, the edge of half-plane 2 is outside the transition region and the observation point is on the shadow boundary of half-plane 2. The GTD formulation can be used to determine the field diffracted from half-plane 1, but this construction fails to provide the correct result for the field diffracted off half-plane 2 along the shadow boundary direction. It actually gives an infinite field which is physically unrealizable. At this point one might be tempted to employ UTD formulation, as in (64), since it would predict a bounded (finite) result. It can be easily verified that UTD formulation does not give the correct asymptotic result when compared with the exact asymptotic solution given in (97). In fact, UTD formulation fails to predict the term χ' in (97).

Two successive applications of MSD and UAT formulations do indeed provide the correct result and demonstrate perfect agreement with (97).

For the situation shown in Fig. 10c, where the edge of half-plane 2 lies at the shadow boundary of half-plane 1 and the observation point is positioned away from the transition region, the GTD formulation obviously fails to determine the field correctly. It is then logical to consider whether or not UTD, MSD or UAT can be applied twice in succession in a cascading fashion to derive the final result. Since the incident field on the half-plane 1 is a plane wave, application of each of the three formulations gives Sommerfeld's solution for the field diffracted by half-plane 1. We can readily show that this field takes the following form at the edge of half-plane 2

$$u_1^t = \frac{1}{2} e^{iks} + \tau\chi_r(\Omega,\Omega)g(ks) + O(k^{-3/2}) \quad . \tag{98}$$

Field (98) can now be viewed as the incident field on half-plane 2. Hence, straightforward (mechanical) application of UTD, MSD and UAT would hopefully provide the field diffracted by half-plane 2 at the observation point. After some simplification, this field takes the following asymptotic form

$$u_2^t = \frac{1}{2} \chi(\Omega,\phi_2)\, e^{iks} g(k\rho_2) + \tau\chi_r(\Omega,\Omega)g(ks)\chi(\Omega,\phi_2)g(k\rho_2) + O(k^{-3/2}) \quad . \tag{99}$$

Comparison of (99) with the correct asymptotic expansion given in (83) reveals that (99) is not complete and misses the term corresponding to $2\chi'(\Omega,\phi_2)$. In other words, straightforward (mechanical) application of UTD, MSD, and UAT does not provide the correct asymptotic result when the edge of half-plane 2 lies at the shadow boundary (transition region) of half-plane 1. This important observation was first made by

Jones [21] for the UAT formulation. Here we have come to a similar important observation that the mechanical application of UTD and MSD does not provide the correct result either. Boersma [22] and Lee and Boersma [19] resolved the difficulty related to UAT by using the argument that the diffracted field (98) from half-plane 1, which varies rapidly in the transition region, does not comply with a ray field behavior. Hence, this field cannot be used directly (mechanically) as the incident field via the application of the UAT formulation. They expanded (98) in terms of an infinite summation of cylindrical and plane waves and applied the UAT formulation to each term of expansion separately. Their final uniform result agrees with Jones' uniform result and with that given in (83).

The difficulties with the straightforward (mechanical) application of UTD, MSD and UAT, as expressed in the preceding paragraph, also exist for the case shown in Fig. 10d. In this case, both the edge of half-plane 1 and the observation point lie at the shadow boundaries. It is straightforward to show that the "mechanical" application of the uniform theories gives

$$u_2^t = \frac{1}{2} e^{ik(s+\rho)} + O(k^{-1}) \tag{100}$$

for the dominant term of the total field. However, the correct dominant behavior is given first in the r.h.s. of (96), which is obviously different from (100). As a matter of fact, as $\rho \to \infty$, (96) gives $(1/2)\exp(iks + ik\rho)$ for the dominant term, i.e., 50 percent different from the "mechanical" result, (100), of the uniform theories. Boersma [22] and Lee and Boersma [19] were able to show that, by carefully analyzing the problem in the manner described earlier, they could obtain the complete result agreeing with (96). However, the same analysis has not yet been performed for the MSD formulation.

5. SPECTRAL DOMAIN APPROACH TO VERIFICATION AND REFINEMENT OF ASYMPTOTIC SOLUTIONS

5.1 Introduction

One of the most challenging problems in the solution of high-frequency scattering analyses is the establishment of the accuracy of the results and the refinement of the solution when the need for its improvement is clearly indicated. The difficulty in verifying whether the asymptotic expression, typically derived from the ray approach, does indeed solve the boundary value problem under consideration stems primarily from the fact that there is no obvious way to "build in" the boundary conditions in solution procedures based on ray methods. Another reason is that the high-frequency solutions are often constructed for the radiated far fields, whereas the application of the boundary conditions clearly requires the near-field information. In contrast, the integral equation formulation for the scattering problem is based directly on the application of the boundary condition and, consequently, the boundary condition check is redundant for this approach. However, the conventional moment method solution of integral equations is limited strictly to the low frequency and resonance regions as the matrix size becomes unmanageably large beyond the resonance region.

In this section we will briefly outline a spectral domain method for bridging the two approaches, viz., the integral equation and asymptotic techniques. The hybrid method has the desirable feature that it not only verifies the accuracy of the ray solutions but provides a systematic means for improving the solution for a large class of problems of practical interest. This fact will be illustrated via two typical examples given in this section. Other cases have also been treated and may be found in [23] and [24].

5.2 Development of Spectral Domain Formulation of the Integral Equation and Its Approximate Solution

The key to combining the asymptotic solution with the integral equation formulation lies in recognizing the fact that the Fourier transform of the induced current on a scatterer is directly proportional to the scattered far field and that a good approximation to this scattered field is often available from any number of asymptotic methods, e.g., GTD or the spectral approach discussed in preceding sections. To take advantage of these facts we choose to work with the "Fourier-transformed" or "spectral domain" version of the integral equation rather than with the conventional spatial domain counterpart of the same equation. We begin, however, with the conventional electric-field integral equation (E-equation) for a perfectly conducting scatterer:

$$(\bar{\bar{G}} * \bar{J})_t = -\bar{E}^i_t \quad , \quad \bar{\bar{G}} = \text{Green's Dyadic} \tag{101}$$

where $\bar{J}(\bar{r}')$ is the unknown induced surface current density, the subscript t signifies the tangential component of the field on the surface S of the scatterer, $\bar{E}^i$ is the incident electric field on the scatterer, and "*" symbolizes the convolution operation.

As a preamble to Fourier transforming (101), we first extend it over all space. To this end we define a truncation operator $\Theta(\bar{A})$.

$$\Theta(\bar{A}) = \int \bar{A}_t \delta(\bar{r} - \bar{r}_s)\, dr \quad , \quad \bar{r}_s \in S \tag{102}$$

where δ is the Dirac delta function. Let $\hat{\Theta}(\bar{A})$ be defined as the complementary operator

$$\hat{\Theta}(\bar{A}) = \bar{A} - \Theta(\bar{A}) \ . \tag{103}$$

Then (101) can be rewritten as

$$\bar{\bar{G}} * \bar{J} = \theta(-\bar{E}^i) + \hat{\theta}(\bar{\bar{G}} * \bar{J}) \tag{104}$$

for all space. Using the definition of the Fourier transform introduced in Sec. 2, now extended to the general three-dimensional case, we can write (104) as

$$\tilde{\bar{\bar{G}}}\tilde{\bar{J}} = -\tilde{\bar{E}}_I + \tilde{\bar{F}} \tag{105}$$

where $\tilde{\bar{F}} = F[\hat{\theta}(\bar{\bar{G}} * (\theta\bar{J})]$ and $\tilde{\bar{E}}_I$ is the transform of the tangential component of the incident field truncated on S, with all transformed quantities being denoted in this section by $\tilde{}$ on top. Note that the convolution operator in the integral equation is transformed into an algebraic product upon Fourier transformation. Note also that (105) has two unknowns, viz., $\tilde{\bar{J}}$ and $\tilde{\bar{F}}$, which must be solved for simultaneously.

At this point one can construct the solution of (105) in at least two ways. The first of these is based on an iterative procedure that begins with an approximation to $\tilde{\bar{J}}$, the transform of the induced surface current, derived from the application of some asymptotic procedure to the scattering problem. The following equation is then employed to generate the next order solution and the procedure is repeated until convergence is achieved:

$$\tilde{\bar{J}}^{(n+1)} = \tilde{\bar{G}}^{-1}\left[-\tilde{\bar{E}}_I + F\left(F^{-1}[\tilde{\bar{\bar{G}}}\tilde{\bar{J}}^{(n)}] - \theta\{F^{-1}[\tilde{\bar{\bar{G}}}\tilde{\bar{J}}^{(n)}]\}\right)\right] \tag{106a}$$

and in the space domain

$$\bar{J}^{(n+1)} = \theta F^{-1}[\tilde{\bar{J}}^{(n+1)}] \quad . \tag{106b}$$

It may be shown that the combination of the second and third terms in (106a) represents an approximation to $\tilde{\tilde{F}}$ derived from the n^{th} approximation of $\tilde{\tilde{J}}$, i.e., $\tilde{\tilde{J}}^{(n)}$. Also, it should be realized that the inverse operator $\tilde{\tilde{G}}^{-1}$ is algebraic since $\tilde{\tilde{G}}$ itself has the same nature. The check for the boundary condition may be readily applied in this procedure since $\mathcal{O}\{F^{-1}[\tilde{\tilde{G}}\tilde{\tilde{J}}^{(n)}]\}$, the last term inside the square bracket in (106a), represents the tangential E-field produced on the surface of the object by the induced current. Ideally, this field should equal the negative of the tangential component of the incident E-field $\bar{E}^i_t$. A comparison between these two fields immediately reveals the extent to which the boundary condition is satisfied on the surface of the scatterer.

A second approach to handling (105) would be to employ the Galerkin procedure in the transform domain. One may write

$$\tilde{\tilde{J}} \simeq \tilde{\tilde{J}}^{(0)} + \sum C_p \tilde{\tilde{J}}_p \tag{107}$$

where $\tilde{\tilde{J}}^{(0)}$ is the approximate solution derived from a suitable asymptotic formula for the scattered field and $\tilde{\tilde{J}}_p$ represents a set of basis functions in the transform domain. Typically, there are certain angular regions in the far field where the asymptotic solutions require refinement. One may choose to concentrate the basis functions in these regions in the transform domain. Alternatively, the $\tilde{\tilde{J}}_p$'s could be chosen as the transforms of a suitable set of basis functions in the space domain, and the location (support) of these subdomain basis functions may be selected to coincide with transition regions or corners, etc., where the canonical solution of the asymptotic solution may require refinement.

In either case, the problem of determining $\tilde{\tilde{J}}$ may be reduced to that of finding the unknown coefficients C_p such that (107) satisfies (105).

The Galerkin procedure provides a way for accomplishing this, as we will soon see. This technique also has the advantage that the other unknown in (105), viz., $\tilde{\tilde{F}}$, is conveniently eliminated from this equation upon application of Galerkin's method. We demonstrate this fact in the manipulations presented below.

Substituting (107) in (105) and taking a scalar product of the resulting equation with a set of suitable series of testing functions $\tilde{\tilde{W}}_q$, we arrive at

$$\sum C_p \langle \tilde{\tilde{W}}_q, \tilde{\tilde{\tilde{G}}} \tilde{\tilde{J}}_p \rangle = -\langle \tilde{\tilde{W}}_q, \tilde{\tilde{E}}_I \rangle + \langle \tilde{\tilde{W}}_q, \tilde{\tilde{F}} \rangle \tag{108}$$

where "$\langle , \rangle$" is the scalar inner product. If we now choose $\tilde{\tilde{W}}_q$ to be transforms of functions which are nonzero only on the surface of the scatterer, then the scalar product $\langle \tilde{\tilde{W}}_q, \tilde{\tilde{F}} \rangle$ can be shown to vanish. To show this, one uses Parseval's theorem and transforms the scalar product of $\tilde{\tilde{W}}_q$ and $\tilde{\tilde{F}}$ in terms of a similar product of their counterparts in the space domain. Since the inverse transforms of $\tilde{\tilde{W}}_q$ and $\tilde{\tilde{F}}$ exist in complementary regions, viz., on the surface of the scatterer and in the region complementary to this surface, respectively, one finds that their scalar product is identically zero. One can now proceed in the usual manner to solve for the coefficients C_p by solving the matrix equation represented by (108) with the second term in the r.h.s. deleted. It is evident that the use of this method would be practical only when relatively few terms are needed in (107) to modify the available asymptotic solution; however, this is typically the situation for many problems. It should also be noted that (108) represents a direct check on the satisfaction of the boundary condition, in the sense of moments. The choice of $\tilde{\tilde{W}}_p$'s is governed by the locations on the surfaces of the scatterer where these

boundary conditions are applied. Typically these will be the zones where the asymptotic solution might be inaccurate, e.g., the transition region between the lit and shadow regions.

5.3 Illustrative Examples

We will now illustrate both the iterative and Galerkin procedures by means of two examples of high-frequency scattering. For the first example we choose the problem of diffraction by a rectangular cylinder, a structure with multiple wedges. The geometry of the problem is shown in Fig. 13. We note that the wedges 1, 2, and 3 and faces A and B are illuminated by the incident wave while the faces C and D and the wedge 4 are in the shadow. Let us first consider the heimsphere above the face A. The contribution to the scattered field in this region comes from the two lit surfaces and rays diffracted by the wedges 1, 2, and 3. To derive a first approximation to the asymptotic expression for the far field scattered by the cylinder, we may use Keller's coefficients for the diffraction by the three wedges. From wedge 1 we have, for instance,

$$H_{z1}^{d} \sim e^{-ik(-a\cos\phi_0+b\sin\phi_0)} \frac{e^{ik\rho}}{\sqrt{\rho}} \frac{e^{i\frac{\pi}{4}}}{\sqrt{2\pi k}} \left\{ \frac{\frac{2}{3}\sin\frac{2\pi}{3}\, e^{ika\cos\phi}\, e^{-ikb\sin\phi}}{\cos\frac{2\pi}{3} - \cos\frac{2}{3}(\phi - \phi_0)} + \frac{\frac{2}{3}\sin\frac{2\pi}{3}\, e^{ika\cos\phi}\, e^{-ikb\sin\phi}}{\cos\frac{2\pi}{3} - \cos\frac{2}{3}(\phi + \phi_0)} \right\} \tag{109}$$

where $0 \leq \phi_0 < \frac{\pi}{2}$ and $0 \leq \phi < 3\pi/2$. Similar expressions can be readily obtained for the wedges 2 and 3. Note that the scattered field from wedge 3 is restricted in the angular region $0 < \phi \leq \pi/2$ and $\pi \leq \phi \leq 2\pi$ for $0 \leq \phi_0 \leq \pi/2$. Hence, in the upper hemisphere only one-half of the angular range is illuminated by the scattered field from wedge 3, if Keller's

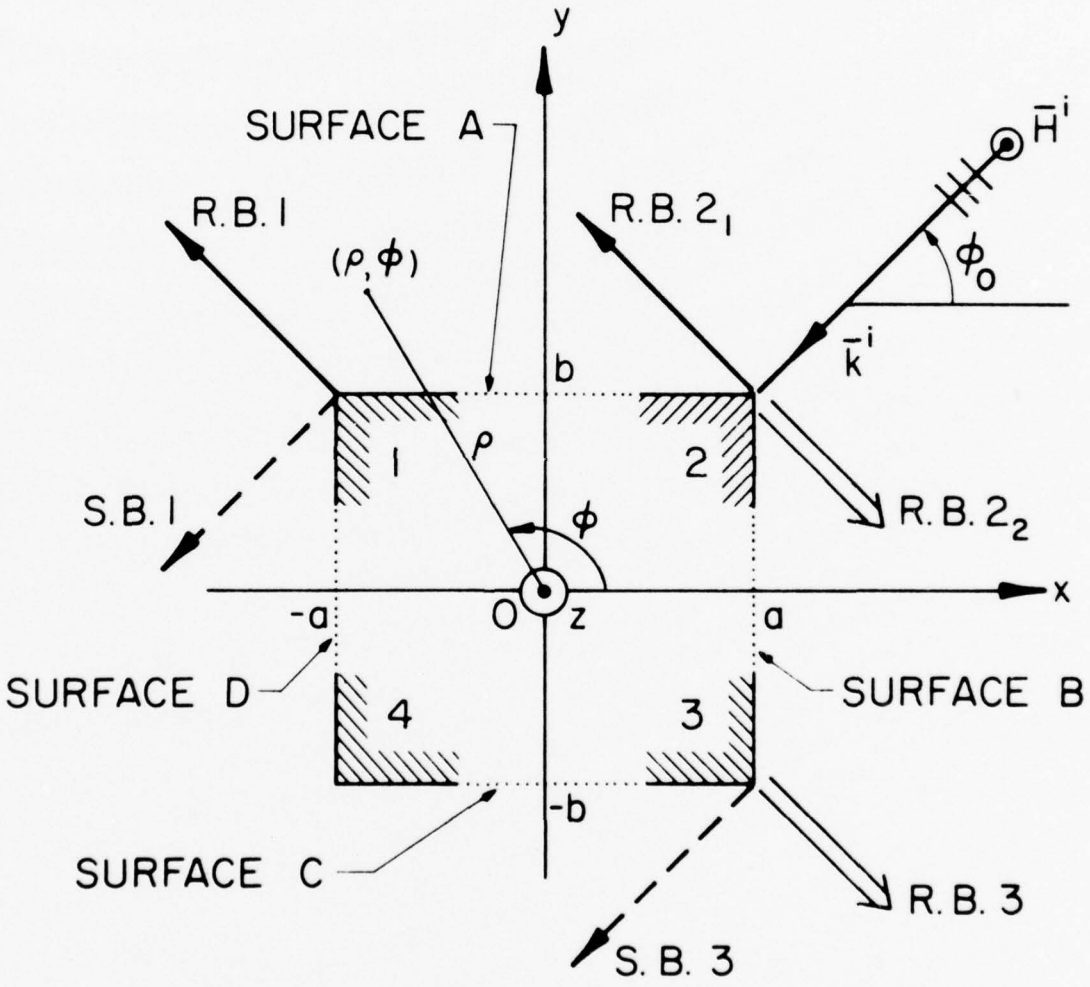

Figure 13. For the angle of incidence ϕ_0 as shown, wedges 1, 2, and 3 are illuminated while wedge 4 is in the dark.

formula for an infinite wedge is used to derive an approximation to this scattered field. Another rather important and common feature of the Keller expressions for the wedge-diffracted fields as given, for instance, by (109), is that these formulas predict fictitious infinities in the scattered fields at the shadow and reflection boundaries. One could completely eliminate these infinities by employing the spectral concepts and deriving the scattered far field from the transform of an approximation to the induced surface current, comprising the physical optics and fringe currents. This transform, being associated with a function with finite support, is always bounded and consequently free of the singular behavior present in (109).

As an alternative we may also employ one of the available uniform theories [17], [14] that provide smooth and bounded transition through the reflection and shadow boundaries. It is fortuitous, however, that the aggregate contribution of the infinities from the individual wedges cancels out exactly when their contributions are superimposed. This occurs because of the unique symmetries of the geometry of the rectangular cylinder under consideration. Hence, no special care is required in this example at the transition regions. The diffracted far fields computed by using the Keller formulas for wedge diffraction are shown in Fig. 14. It is evident that the pattern is discontinuous at 0°, 90°, 180°, and 270°. This behavior is attributable to the use of infinite wedge diffraction coefficients that produce a nonzero scattered field only in the region external to the wedge and, hence, produce discontinuous fields supported by induced surface currents that extend to infinity along the wedge surfaces.

To refine this far-field asymptotic solution, we may now proceed to apply the iterative procedure developed in Sec. 5.2. To this end, we first introduce in Fourier transform the variable $\alpha = k \cos \phi$ and express

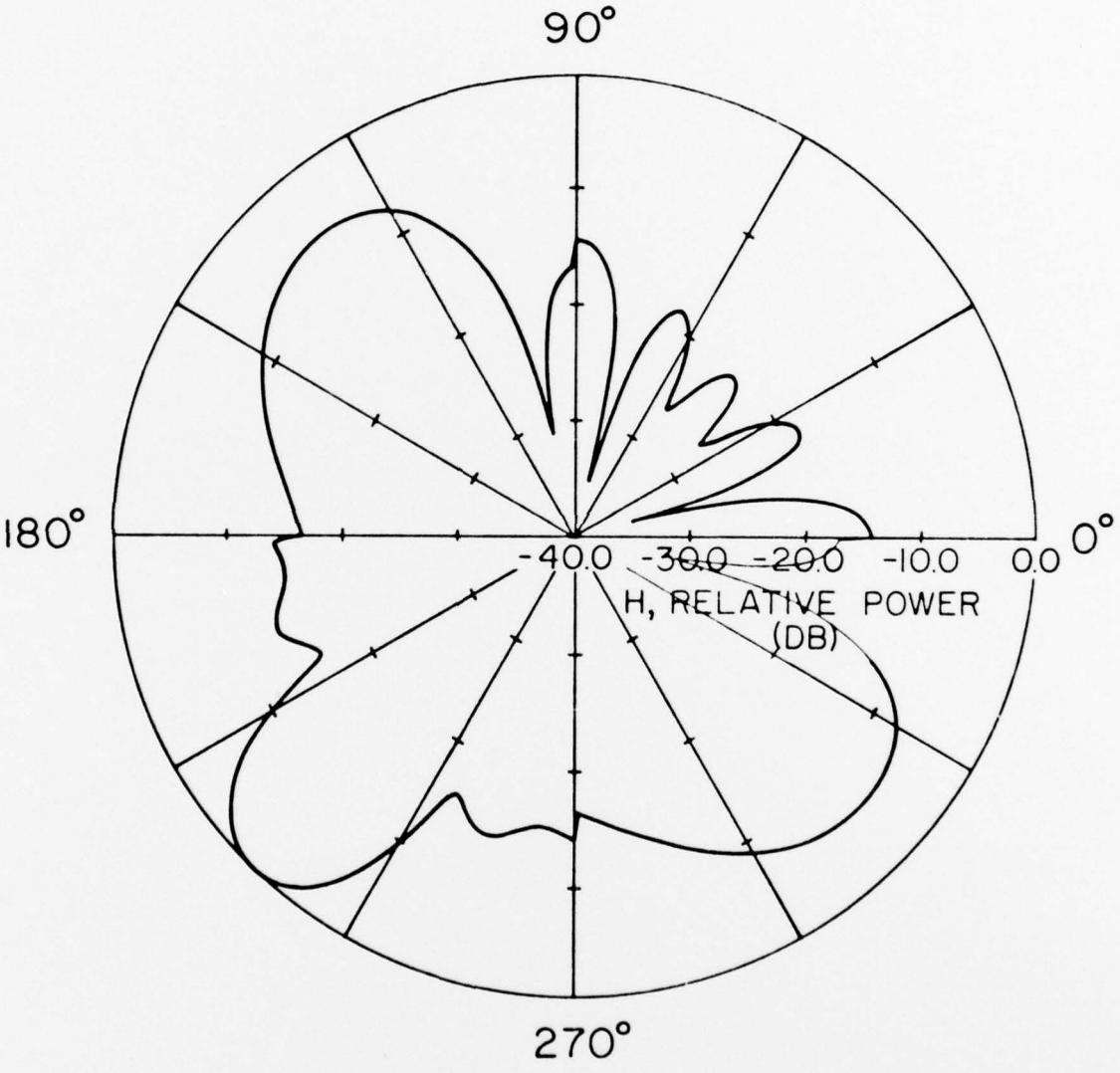

Figure 14. GTD diffracted far-field pattern of the rectangular cylinder; $\phi_0 = \pi/4$, $a = b = 1\lambda$.

the far scattered field in the hemispherical region defined by $0 < \phi < \pi$ in terms of α. We employ analytical continuation of the expressions for the wedge-diffracted fields to determine the Fourier transform in the range $|\alpha| > k$ by substituting appropriate complex values for ϕ. One of the chief advantages of using the available expressions for the asymptotic solution as a starting point for the iterative procedure is that the approximate analytical expression is convenient for estimating the scattered far field, both in the visible and invisible ranges. By Fourier inversion of the scattered E-field at infinity, we can derive the tangential E-field on a planar surface tangential to the face A. If this computed near field were to satisfy the boundary condition that the tangential E-field on surface A equal the negative of $\bar{E}^i$, and the similar situation is repeated for other faces, we would conclude that the solution so derived is an accurate one. However, we would not expect that to be true for the solution represented by (109) since, as pointed out earlier, this expression produces glitches at some angles of observation. Nevertheless, this solution provides a very good zero order estimate for $\tilde{\bar{F}}^{(0)}$ which is readily derived by taking the transform of the near field derived in the plane of the surface A, after deleting the portion of the field that corresponds to the surface A of the scatterer, and repeating the same procedure for the other faces as well. In following this procedure, we effectively compute

$$F\left\{F^{-1}[\tilde{\bar{\bar{G}}}\tilde{\bar{J}}^{(0)}] - \Theta\{F^{-1}[\tilde{\bar{\bar{G}}}\tilde{\bar{J}}^{(0)}]\}\right\}$$

which is an approximation to $\tilde{\bar{F}}$ derived by using $\tilde{\bar{J}}^{(0)}$. The next order of approximation to $\tilde{\bar{J}}$ is now readily obtained from (106). This quantity is Fourier inverted four times to calculate the tangential H-field on the

four faces of the cylinder and the surface current on these faces, obtained from (106b), is Fourier transformed again to derive the far-field pattern.* The iterated far-field pattern $\bar{J}^{(1)}$ is shown in Fig. 15; the disappearance of the discontinuities at 0, $\pi/2$, $3\pi/2$, etc., is immediately evident from this plot. This result has also been verified by a few other workers who have followed different procedures than those outlined here [25]. Recall, however, that the method outlined here provides a convenient "built-in" check for the satisfaction of the boundary condition and an independent check is not altogether necessary to establish the accuracy of the solution.

The next example we discuss is that of a smooth convex surface with no wedges — a circular cylinder. One of the important attributes of this canonical geometry is that it permits convenient comparison with the exact series solution available for the representation of scattered fields from this structure. The geometry of the problem is shown in Fig. 16. We consider the case of an E-polarized wave incident from $\phi = 180°$.

The first step in attacking the problem is to use a geometrical optical (60) approach) [24] to derive the far-scattered field. When this is done, one obtains the dotted curve in Fig. 17 which also exhibits the exact series solution for the scattered field as a solid curve. It is evident that in the range $-60° < \phi < 60°$ the GO solution is not adequate. This is not totally surprising since it is well-known that creeping-wave contributions need to be included in the scattered field expression in the shadow and transition regions. Rather than following this procedure, we will now show how the Galerkin method can be readily and conveniently applied to this problem to derive an accurate solution.

---

* Numerical experiments have shown that very good far-field results are obtained even when one skips the first step and uses $\bar{J}^{(0)}$ itself to derive the surface current using (106b) and $\bar{J}^{(1)}$ by the Fourier transformation of this current.

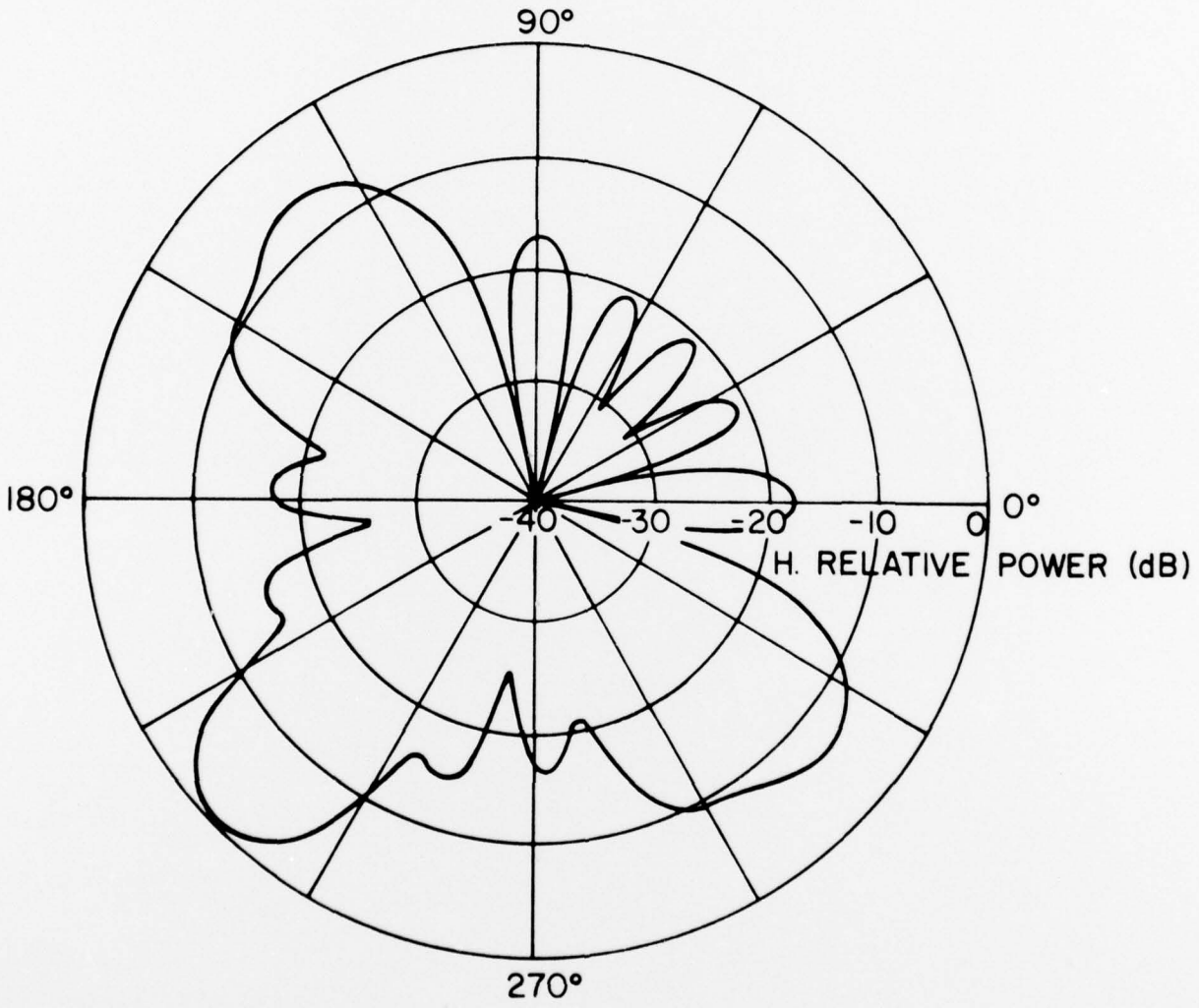

Figure 15. Improved scattered far-field pattern of the rectangular cylinder; $\phi_0 = \pi/4$, $a = b = 1\lambda$.

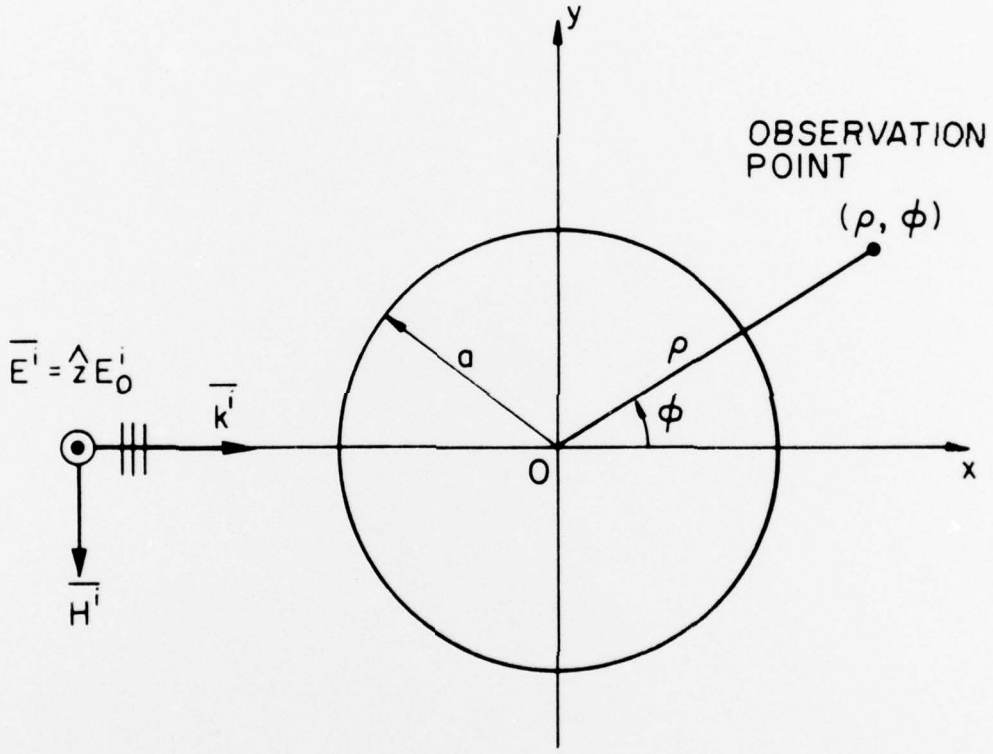

Figure 16. Diffraction by a circular cylinder illuminated by an E-wave incident along the x-axis.

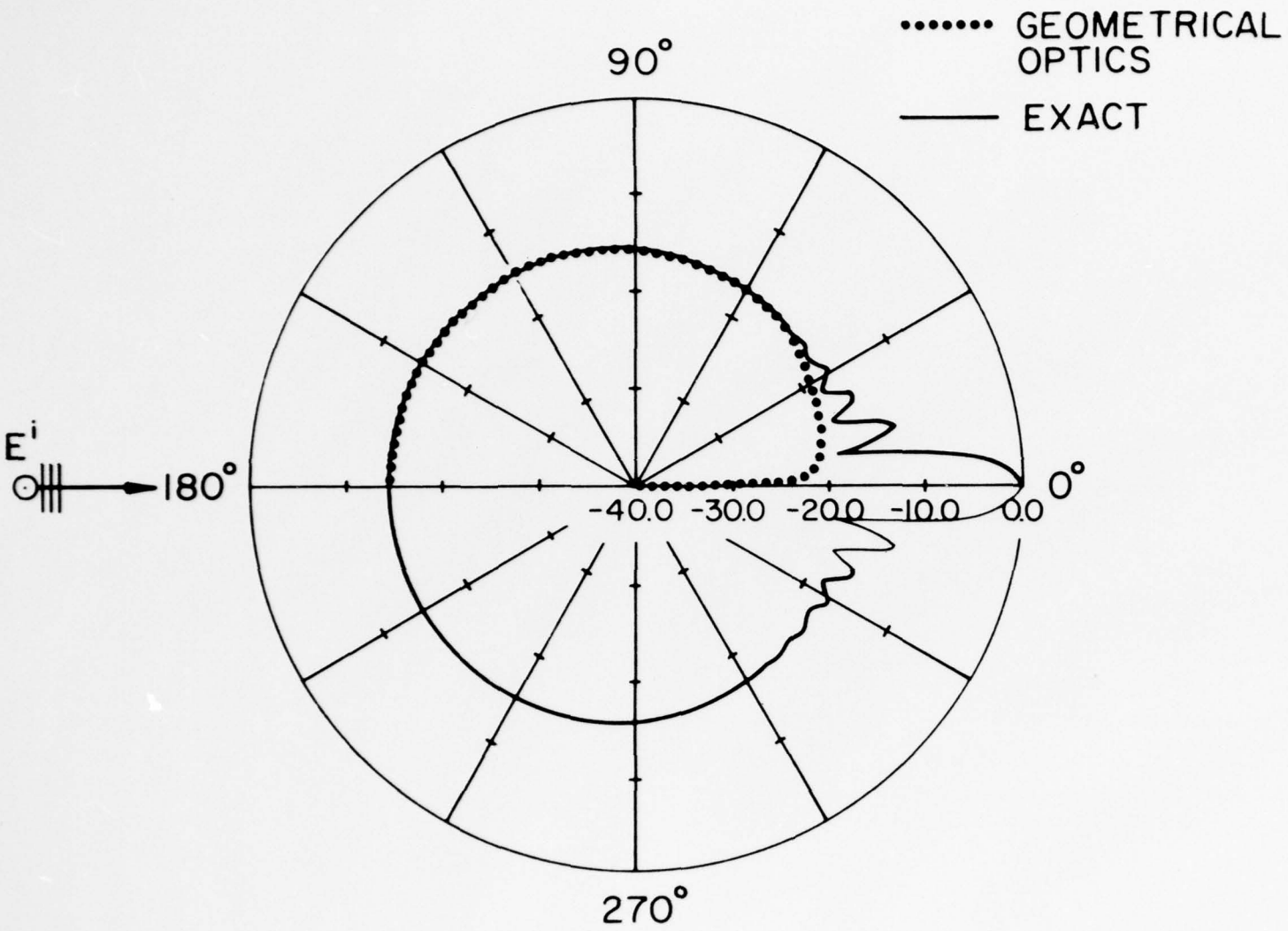

Figure 17. Geometrical optics scattered far-field pattern in dB of a circular cylinder with radius a = 3λ.

To this end we consider, as a first step, the behavior of the scattered field on a surface erected in juxtaposition to the cylinder at the point $x = a$, the farthest point away from the incident field. In the deep shadow region, say $|y| < 2$, we expect the scattered field $E_z^s = -E_z^i$ to be a very good approximation. On the other hand, when we go far onto the lit region on this surface, say for $|y| > 6$, we expect the E_z^s to be described adequately by the GO formulas. If we had a good estimate of the scattered field behavior in the transition region $2 < |y| < 6$, we would be able to get a good representation of the excess scattered field (over and above the GO field) on the entire surface at $x = a$. We should then be able to compute the field radiated in the r.h.s. of the cylinder by this excess field using the concept of Huyghen's source and use this radiated field to fill in the gap between the GO pattern and the true pattern shown in Fig. 18.

To derive the E_z^s field in the transition region, we first interpolate the magnitude of this field from E^i at $|y| = 2$, to 0 at $y = 6$ and the phase from π at $|y| = 2$, to the GO phase at $|y| = 6$. Next we introduce a set of basis functions, with undetermined coefficients, to describe the correction to the interpolated E_z^s field at the plane $x = a$, $2 < |y| < 6$. To determine these coefficients, we apply the concept of Galerkin's method in the spectral domain as briefly outlined in Sec. 5.2. In the example being considered here, the transforms of the basis functions play the role of $\tilde{\bar{J}}_p$ in (107), and the zero-order, scattered far field $\tilde{\bar{J}}^{(0)}$ is obtained by adding the contributions of GO and the approximate excess E_z^s field derived from the interpolation procedure just described.

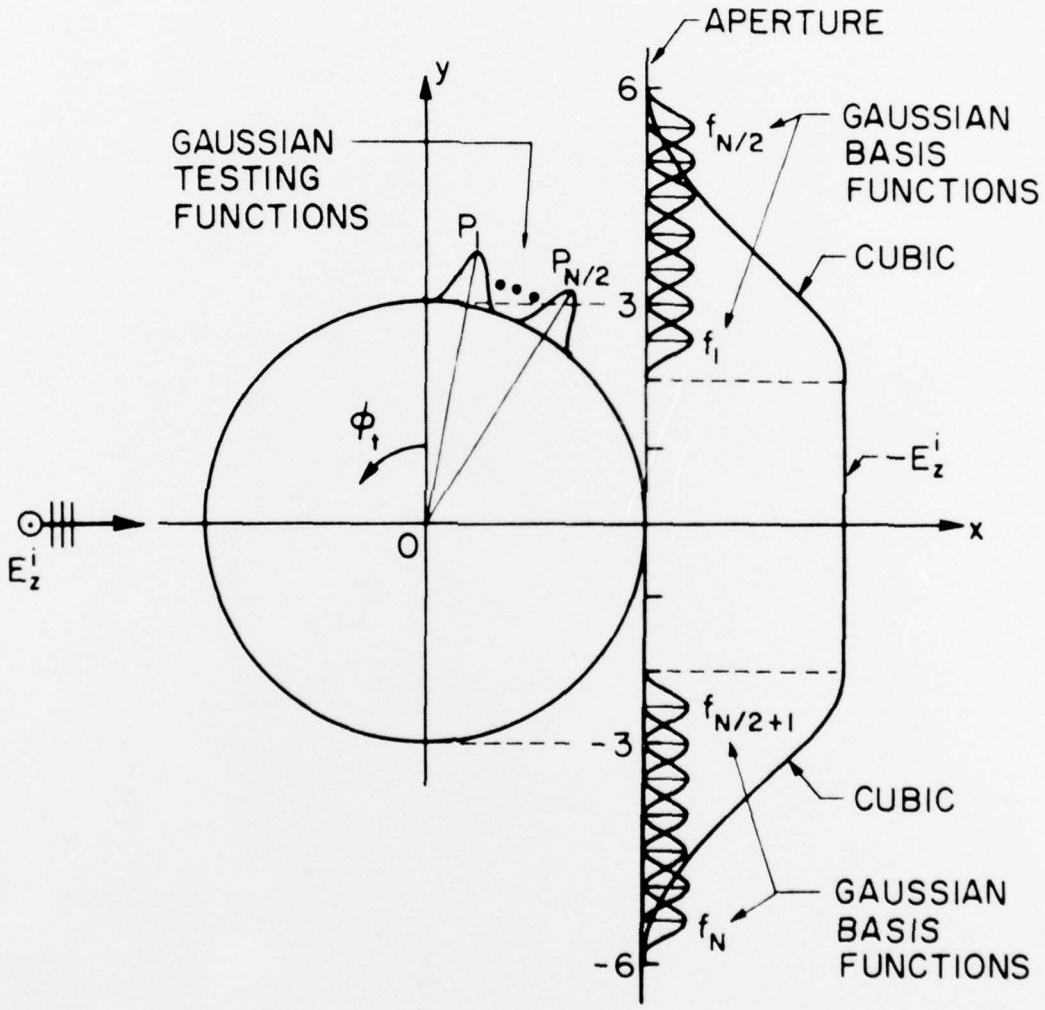

Figure 18. Locations of the basis functions on the aperture and the testing functions on the surface of the obstacle.

The choice of the testing functions, $\tilde{\tilde{W}}_q$ in (108), is suggested by the fact that the error in the high-frequency asymptotic solution is mostly concentrated around the transition region on the surface of the cylinder, i.e., in the neighborhood of the junction between the lit and shadow regions. Thus, a suitable choice for the testing functions would be to locate them at the transition region as shown in Fig. 18 where the location of the basis functions is also shown. Note that we need not be restricted in our choice for the location of these functions by demanding that they have a common support, although this is almost always the case in the conventional moment or Galerkin methods. We may also note from Fig. 18 that the shape of the basis and testing functions are both Gaussian. Since we are dealing with transforms, this choice is not only convenient for deriving the Fourier transformations $\tilde{\tilde{J}}_p$ and $\tilde{\tilde{W}}_q$, but is also desirable from a numerical point of view because the transforms are not oscillatory as they would be for a pulse or triangular basis. This feature is important when numerically computing the scalar products $<\tilde{\tilde{J}}_p, \tilde{\tilde{W}}_q>$, needed for the determination of the unknown coefficients C_p.

Only a few unknowns C_p (3 to 7) are needed to derive an accurate solution for both the radiated far field and the surface current on the cylinder. The accuracy itself can be verified by computing the tangential E-field on the surface via Fourier inversion of the hemispherical far-field pattern centered around the point to be tested. This procedure is also used to compute the surface current distribution from the knowledge of the scattered H-field at large distances. Of course an independent check is available for this problem via the exact series solution. A comparison of the Galerkin solution and the exact series solution is shown in Figs. 19 and 20 to illustrate the highly accurate nature of the

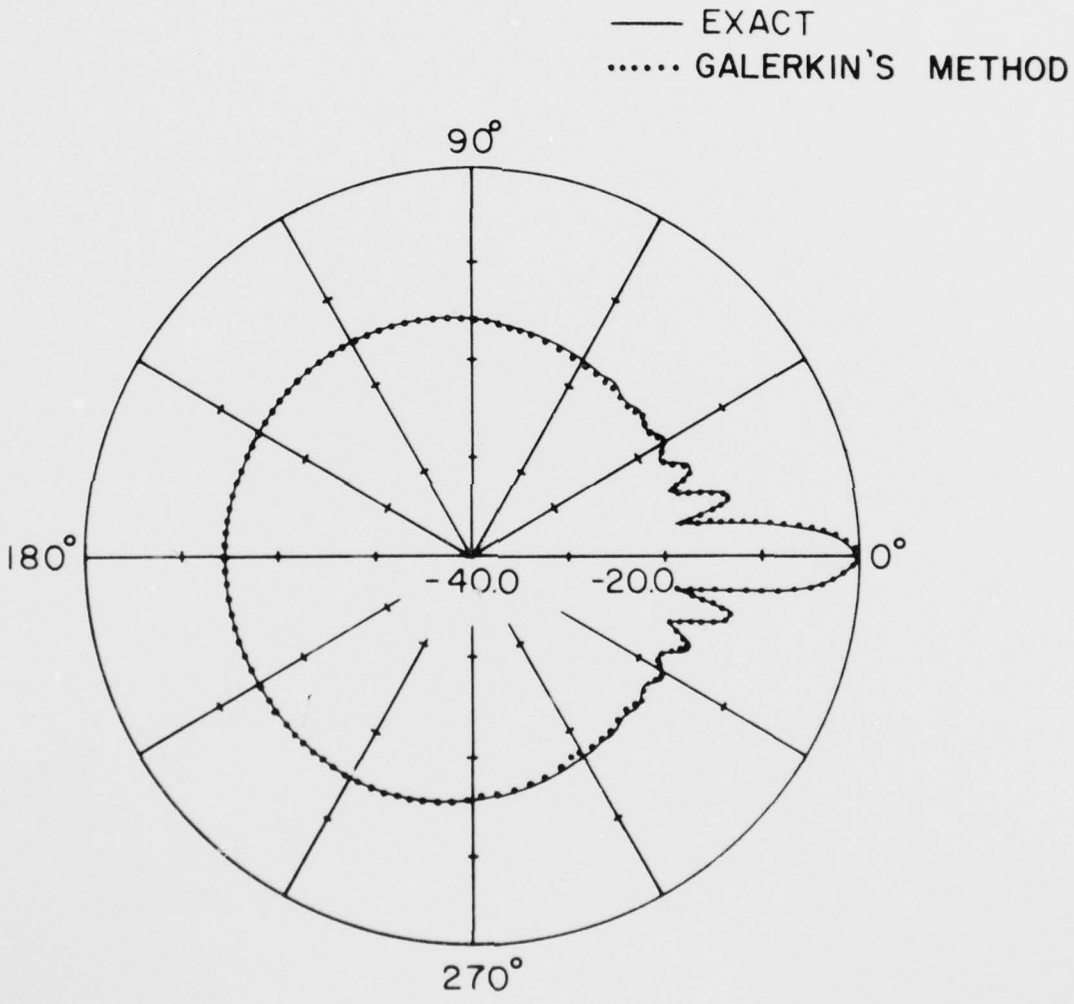

Figure 19. Scattered far-field pattern in dB of a circular cylinder with radius a = 3λ obtained by Galerkin's method.

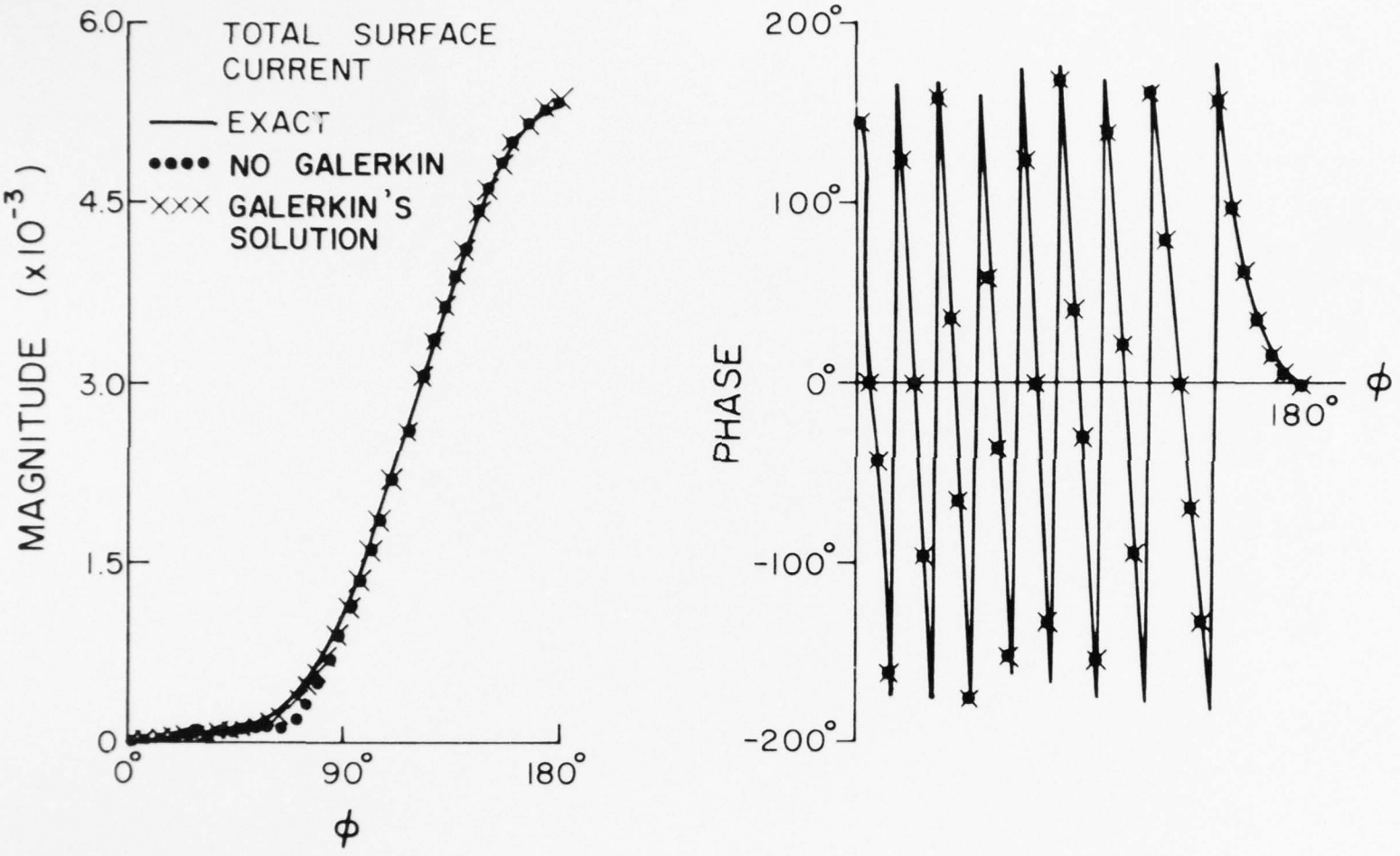

Figure 20. Total surface current on a perfectly conducting circular cylinder with radius a = 3λ.

Galerkin solution. In fact, the solution is surprisingly accurate, except for a slight error in the transition region, even without the Galerkin refinement, as evidenced by the dotted curve in Fig. 20 which exhibits this case.

The method just described could easily be employed for more complex, nonseparable shapes as long as the smooth convex nature of the surface is preserved. A generalization to even more complex geometries, e.g., combination of curved surfaces and wedges, also appears possible.

REFERENCES

[1] J. B. Keller, "Geometrical theory of diffraction," J. Opt. Soc. Am., vol. 52, pp. 116-130, 1962.

[2] R. G. Kouyoumjian, "The geometrical theory of diffraction and its application," in Topics in Applied Physics, vol. 3, R. Mittra, Ed. New York: Springer Verlag, 1976, pp. 165-215.

[3] R. Mittra, Y. Rahmat-Samii and W. L. Ko, "Spectral theory of diffraction," Appl. Phys., vol. 10, pp. 1-13, 1976.

[4] B. Noble, Methods Based on the Wiener-Hopf Technique. London: Pergamon Press, 1958.

[5] M. Born and E. Wolf, Principles of Optics. New York: Macmillan, 1964.

[6] R. Mittra and S. W. Lee, Analytical Techniques in the Theory of Guided Waves. New York: Macmillan, 1971.

[7] G. A. Deschamps, "Ray techniques in electromagnetics," Proc. IEEE, vol. 60, pp. 1022-1035, 1972.

[8] Y. Rahmat-Samii and R. Mittra, "A spectral domain interpretation of high-frequency diffraction phenomena," to be published in IEEE Trans. Antennas Propagat., 1977.

[9] P. C. Clemmow, The Plane Wave Spectrum Representation of Electromagnetic Fields. Oxford: Pergamon Press, 1966.

[10] Y. Rahmat-Samii and R. Mittra, "Spectral analysis of high frequency diffraction of an arbitrary incident field by a half-plane — comparison with four asymptotic techniques," University of Illinois at Urbana-Champaign, Electromagnetics Laboratory Technical Report No. 76-10, November 1976.

[11] P. C. Clemmow, "A note on the diffraction of a cylindrical wave by a perfectly conducting half-plane," Quart. J. Mech. Appl. Math., vol. III, (3), pp. 377-384, 1950.

[12] R. Kh. Khestanov, "Diffraction of an arbitrary field at a half-plane," Radio Eng. Electron. Phys. (USSR), vol. 15, pp. 250-256, 1970.

[13] J. Boersma and S. W. Lee, "High-frequency diffraction of a line-source field by a half-plane, Part I. Solutions by ray techniques," to appear.

[14] D. S. Ahluwalia, R. M. Lewis and J. Boersma, "Uniform asymptotic theory of diffraction by a plane screen," SIAM J. Appl. Math., vol. 16, pp. 783-807, 1968.

[15] L. B. Felsen and Marcuvitz, Radiation and Scattering of Waves. Englewood Cliffs, New Jersey: Prentice-Hall, 1973.

[16] S. W. Lee and G. A. Deschamps, "A uniform asymptotic theory of electromagnetic diffraction by a curved wedge," IEEE Trans. Antennas Propagat., vol. AP-24, pp. 25-34, January 1976.

[17] R. G. Kouyoumjian and P. H. Pathak, "A uniform geometrical theory of diffraction for an edge in a perfectly conducting surface," Proc. IEEE, vol. 62, pp. 1448-1461, 1974.

[18] Y. M. Hwang and R. G. Kouyoumjian, "A dyadic coefficient for an electromagnetic wave which is rapidly varying at an edge," URSI 1974 Annual Meeting, Boulder, Colorado.

[19] S. W. Lee and J. Boersma, "Ray-optical analysis of fields on shadow boundaries of two parallel plates," J. Math. Phys., vol. 16, pp. 1746-1764, 1975.

[20] P. Wolfe, "Diffraction of plane waves by a semicircular strip," Quart. J. Mech. Appl. Math., vol. 28, pp. 355-371, 1975.

[21] D. S. Jones, "Double knife-edge diffraction and ray theory," Quart. J. Mech. Appl. Math., vol. 26, pp. 1-18, 1973.

[22] J. Boersma, "Diffraction by two parallel half-planes," to appear in Quart. J. Mech. Appl. Math..

[23] W. L. Ko and R. Mittra, "A new approach based on a combination of integral equation and asymptotic techniques for solving electromagnetic scattering problems," IEEE Trans. Antennas Propagat., vol. AP-24, March 1977 (in press).

[24] W. L. Ko and R. Mittra, "A method for combining integral equation and asymptotic techniques for solving electromagnetic scattering problems," University of Illinois at Urbana-Champaign, Electromagnetics Laboratory Technical Report No. 76-6, May 1976; prepared under Contracts DAHC04-74-G-0113 and N00014-75-C-0293.

[25] W. D. Burnside, C. L. Yu and R. J. Marhefka, "A technique to combine the geometrical theory of diffraction and the moment method," IEEE Trans. Antennas Propagat., vol. AP-23, pp. 551-558, July 1975.